Article

Effective Removal of Nile Blue Dye from Wastewater using Silver-Decorated Reduced Graphene Oxide

Natasha, Abbas Khan,* Ubaid Ur Rahman, Sadaf, Muhammad Yaseen, Rasha A. Abumousa,
Rozina Khattak, Noor Rehman, Mohamed Bououdina, and Muhammad Humayun*

Read Online

ACCESS | Metrics & More | Article Recommendations

ABSTRACT: Nile blue (NB) dye is a highly toxic substance that when discharged into sewage presents a significant risk to the environment and human health. Carbon-based nanomaterials, such as graphene oxide (GO), reduced graphene oxide (rGO), and their nanocomposites, offer considerable potential for eliminating hazardous pollutants from aqueous systems. In this study, we have successfully fabricated bare GO and rGO, and then, the rGO was decorated with silver (Ag) nanoparticles to develop the Ag-rGO composite. The as-prepared materials were characterized by various techniques, such as UV−visible (UV−vis) and Fourier transform infrared (FTIR) spectroscopies, X-ray diffraction (XRD), energy-dispersive X-ray (EDX), and scanning electron microscopy (SEM) to elucidate their structure, morphology, and chemical composition. The pollutant removal performance of the as-prepared materials was evaluated through a batch approach under the effect of various experimental variables for removal of NB dye from wastewater. As obvious, the Ag-rGO composite revealed exceptional performance for NB dye removal from wastewater, with a maximum removal percentage of 94% within 60 min, which is remarkably higher than those of the rGO (i.e., 59%) and GO (i.e., 22%), under the same experimental conditions. The adsorption data was analyzed with thermodynamics, isotherms, and kinetics models to better understand the physicochemical mechanisms driving the effective removal of the NB dye. The results reveal that Ag-rGO nanocomposite exhibit excellent adsorption ability as well as favorable thermodynamic and kinetic parameters for NB dye removal. It was also found that the presence of light enhanced the adsorptive removal of NB while using Ag-rGO as an adsorbent. The present study noted significant reusability of the Ag-rGO nanocomposite, likely due to minimal Ag leaching and/or the robust stability of the Ag-rGO. It is suggested that Ag-rGO-based hybrid materials could serve as promising candidates for efficiently adsorbing and catalytically removing various toxic pollutants from wastewater.
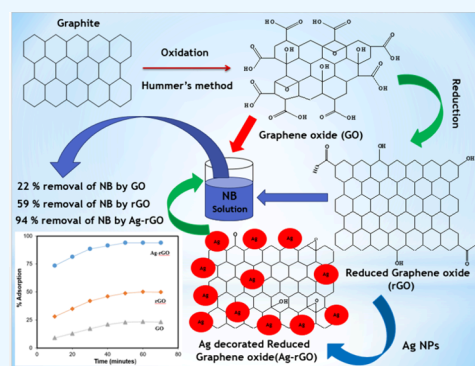
1. INTRODUCTION

Water pollution remains a significant global challenge,[1] with the increasing need for clean water. Advanced techniques for removing heavy metal ions, organic dyes, and microcontaminants from wastewater have been widely explored in recent times.[2] Various materials, including activated carbon, carbon nanotubes (CNTs), metal−organic frameworks (MOFs), MXenes, covalent organic frameworks (COFs), MoS_2, transition metal dichalcogenides, and polymers, have been investigated for water purification and other separation applications. However, their performance in widespread industrial applications has been found to be ineffective over time.[3−5] The exceptional properties of carbon and its composite materials have gotten significant scientific attention for applications in energy and the environment.[6] Graphene, which is a hexagonally packed two-dimensional monolayer of carbon atoms,[3] has captured considerable interest because of its unique electronic structure, and graphene has remarkable

physical properties and has attracted tremendous fascination for researchers in both scientific and engineering disciplines.[7,8] Furthermore, graphene, along with its byproducts GO and rGO, is one of the most well-known carbon compounds.[9] Graphene oxides have more recently been recognized as unique carbon-based nanoparticles with special properties, such as a high volume-to-surface area ratio and a low production cost. Coupling of GO and rGO could remarkably improve the photocatalytic performance of semiconductor-based catalysts. The GO and rGO can be strengthened with functional groups or metal nanoparticles (like silver, platinum,

palladium, gold, copper, and titanium oxide) to form G-based composite materials.[10,11] Silver is a viable option for modifying graphene due to its low price, optical properties, chemical inertness, and nontoxicity. Nanosilver applications include bandages, biomaterials, medicine, water purifiers, and textile manufacturing.[12] Reprocessing wastewater after pollution treatment is essential for water safety. Contamination of water resources is increasing due to population growth.[13] The dissolved organic dyes in the textile industry wastewater impart specific color to the water. Every year, millions of tons of azo dyes, characterized by the presence of $-N\equiv N-$ functional groups in their molecular structure, are produced.[14,15] Among synthetic dyes, azo dyes are the most common type, playing a significant role in the manufacturing of food, paper, paint, pharmaceuticals, cosmetics, leather, and textiles.[16] Nile blue is a synthetic azo dye that is used in textiles and has been proven to cause irritation, lung cancer, allergic eye responses, and inflammation of the skin. Before being disposed of in water, industrial wastewater must be carefully treated.[17] Therefore, to mitigate its harmful impact, it is imperative to eliminate Nile blue (NB) from the environment. A variety of treatment methods, such as coagulation, filtration, erosion, ultrafiltration technology, adsorption, and advanced oxidation procedures (AOPs), have been used to eliminate color dyes from wastewater.[18] These techniques are costly and less effective in eliminating dyes, resulting in secondary pollution issues. Consequently, the removal of dyes from the environment has become increasingly challenging. Despite these limitations, adsorption remains a favored method among researchers due to its straightforward approach, high effectiveness, simple recovery process, and adaptability. Additionally, adsorbents can be reused multiple times, and any hazardous byproducts formed during degradation can be eradicated.[19] Furthermore, several nanomaterial-based adsorbents have been used for pollutant adsorption, comprising porous materials, activated carbon, polymer adsorbents, GO, zeolite, CuO, ZnO, and silica. Particularly, nanomaterials based on metal decorated reduced graphene oxide adsorbents such as Pt/rGO,[20] Au/rGO,[21] Ag/rGO,[22] Fe/rGO,[23] Pd/rGO[24] have captured researcher's attention due to the exceptional adsorption performance, synergistic effects, selectivity, tailorable properties, and versatility. In a recent study, Mondal et al. synthesized an Ag/rGO composite via a green synthesis method. The adsorbent was utilized for the removal of naproxen (NPX), showing a removal efficiency of 92.62% for the NPX anions from contaminated solutions.[25] Metal-decorated rGO-based adsorbents exhibited good adsorption efficiency for the removal of Direct Blue-14 (DB-14) dye.[19] Likewise, fabricated Ag/rGO-based materials show good removal efficiencies for methylene blue (MB) dye[26] and ethylene blue dye.[27] Kamali et al. investigated that Zeolite clay/Fe−Al LDH adsorbent exhibited 99.15 and 98.16% adsorption efficiencies toward the adsorption of methyl violet (MV) and Nile blue (NB) dyes, respectively.[28] Some other adsorbents, such as MoO3/Ppy prepared through the oxidative polymerization of pyrrole monomer with MoO_3 nanoparticles, also exhibit good adsorption efficiency for removing Cd^{2+} and Nile blue (NB) from aqueous solutions.[29] Foroutan et al. also synthesized CNT/MgO/CuFe2O4 composites and evaluated their role as adsorbents; it was observed that the materials exhibit efficient removal efficiency for methyl violet (MV) and Nile blue (NB) dyes.[30] Some other pollutants such as methylene blue (MB), crystal violet (CV), Nile blue (NB), Congo red (CR), As(III),

and As(V) were also removed through adsorption using Ni−Co−S@Ct as the adsorbent.[31] Alali et al.[32] fabricated hydroxyapatite@Mn−Fe composite and utilized as an adsorbent for the removal of NB. It was studied in the light of their results that the adsorbent showed 98.83% for NB dye at pH 10. In another report by Chowdhury et al.,[33] investigated a superadsorbent Ni−Co−S/SDS using a facile method and confirmed through the results that the materials exhibited an adsorption capacity of 4417.79 mg g^{-1} for NB and an adsorption efficiency higher than 95%. Du et al. studied the adsorption of Pb(II) ions from wastewater using hydrothermally fabricated MoS2/rGO composites.[34] In another study, it was found that MoS_2/rGO composite exhibited better efficiency (75.9%) in the removal of Cr(VI) compared to bulk MoS_2 (61.0%).[35] Abedinpour et al. synthesized various heterostructure composite materials, including MoS_2/rGO, MoS_2/Fe3O4/rGO, and Fe3O4/MoS_2/rGO, which were utilized as adsorbents for removing pollutants such as 2-nitroaniline (2-NA) and 4-nitroaniline (4-NA).[36] Trang et al. also discovered that MoS_2/rGO composite materials exhibit significant activity in adsorbing RhB dye.[37] These graphene-based heterostructural materials (MoS_2/rGO) also acted as good adsorbents for the removal of methylene blue (MB)[38] and perfluorooctanoic acid (PFOA).[39] Similarly, some other effective adsorbents for the removal of NB dye comprising AC/CoFe2O4,[40] double-oxidized GO sheets coated polydopamine,[41] MoO_3/polypyrrole composite,[29] CNT/MgO/CuFe2O4 magnetic nanocomposite,[30] clay/starch/MnFe2O4 magnetic composite,[42] zeolite clay/Fe−Al hydrotalcite nanocomposite,[43] La-doped MoS_2 nanosheets,[44] GO-decorated CaO quantum dots,[45] and so forth were reported. Furthermore, composites such as chitosan−MgO,[46] chitosan−Al2O3, magnetic pectin−iron oxide,[47] magnetic EDTA-modified chitosan−SiO2−Fe3O4,[48] guar gum-nZnO,[49] Ppy/SiO2, Ppy/Al2O3, Ppy/Fe3O4,[50] Ppy/CNTs-CoFe2O4,[51] Ppy/TiO2[52] and so forth have been previously synthesized and utilized by various researchers as adsorbents for removing metals and dyes from wastewater.

To the best of our knowledge and based on the literature mentioned above, only a few studies have been reported on the fabrication and environmental applications of Ag-rGO composites. However, there are still numerous aspects to explore in this field. Therefore, in this article, we present the fabrication, characterization, and adsorptive application of Ag-rGO nanocomposites. The as-prepared composite was utilized for the adsorption of Nile blue dye under the effect of various experimental variables as well as under the dark and photoassisted approaches. The composite revealed exceptional performance for NB dye (20 mg/L) removal from wastewater, with a maximum removal percentage of 94% within 1 h, which is far greater than those of the pristine rGO and GO-based materials. The adsorption data was analyzed with thermodynamics, isotherms, and kinetics models to better understand the physicochemical mechanisms driving the effective removal of NB dye. It is also expected that determining the thermodynamic and kinetic parameters for the fabricated Ag-rGO nanocomposite in the removal of NB may also help extend the application of these hybrid materials to a variety of adsorption and catalysis processes from an environmental perspective in the future.

Scheme 1. Schematic Representation for the Synthesis of Graphene Oxide (GO)
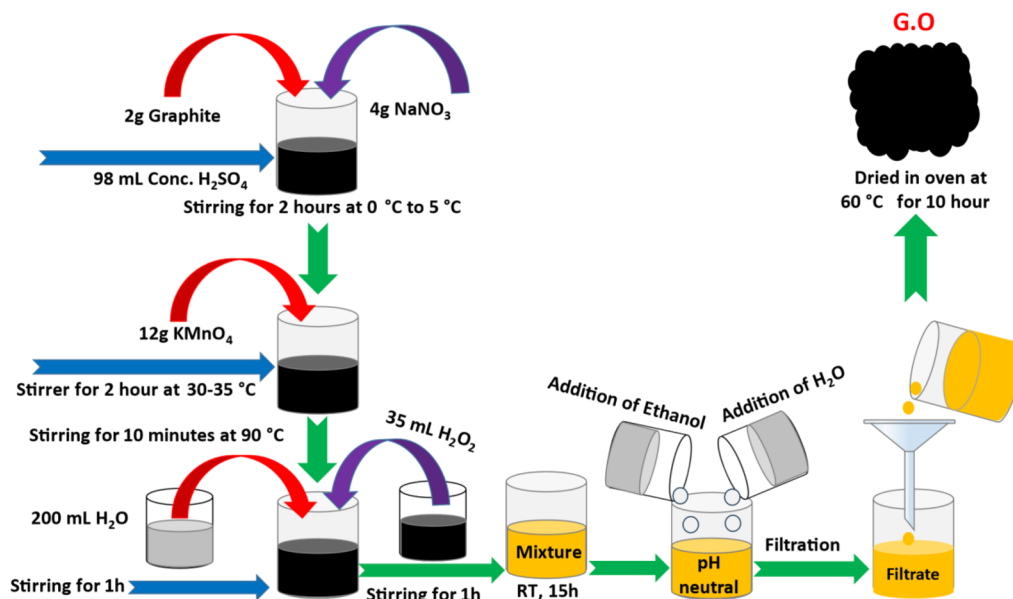
Scheme 2. Schematic Representation of the Preparation of Reduced Graphene Oxide (rGO)
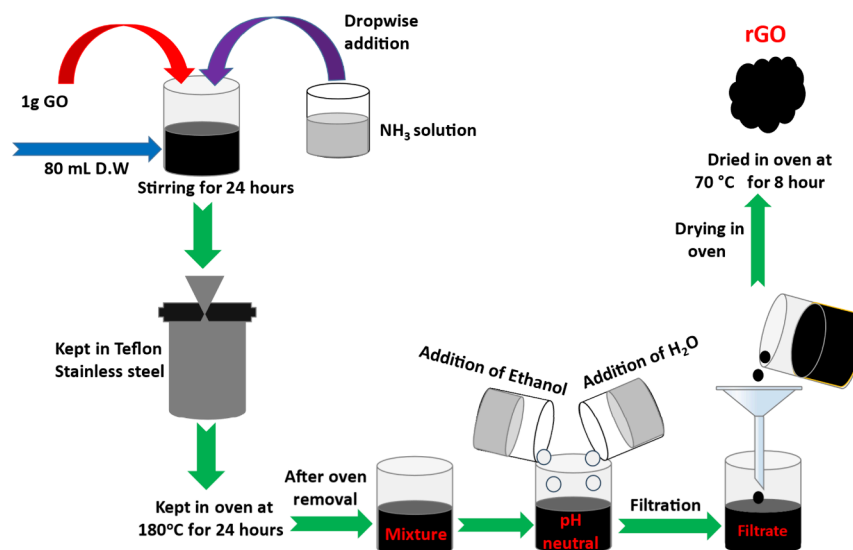

2. EXPERIMENTAL SECTION

2.1. Chemicals and Apparatus. The chemicals and reagents used in this work include graphite (Sigma-Aldrich, 99%), sodium nitrate (Sigma-Aldrich, 99.99%), sulfuric acid (Sigma-Aldrich, 95−97%), potassium per magnate (Sigma-Aldrich, ≥ 99.0%), hydrogen peroxide (Sigma-Aldrich, 30% (w/w) in H_2O), silver nitrate (Sigma-Aldrich, 99.99%), hydrazine hydrate (Sigma-Aldrich, 24−26%), sodium hydroxide (Sigma-Aldrich, reagent grade, 97%), fuming hydrochloric acid (Sigma-Aldrich, 37%), ethanol (Sigma-Aldrich,absolute, ≥ 99.8%), nitric acid (Sigma-Aldrich, 70%), ammonia (Sigma-Aldrich, anhydrous, ≥ 99.95%), and Nile blue dye (Sigma-Aldrich, 95%). Deionized water was used throughout experiments. All the chemicals were of high purity and purchased from Sigma-Aldrich supplier. The equipment used in this project include digital balance, hot plate with magnetic stirrer, drying oven, digital orbital shaker, Teflon-lined autoclave, centrifuge (Eppendorf, Model 5804R), pH meter (Thermo Fisher), UV−C light, ultraviolet−visible (UV−vis) spectrophotometer(PerkinElmer, Lambda 35), X-ray diffraction (XRD, Bruker-D8 Advance), scanning electron microscopy (SEM, JEOL-JSM-7001F), energy-dispersive X-rays (EDX, JEOL), and Fourier transform infrared (FTIR, PerkinElmer-100 FT-IR, USA) spectrometer.

2.2. Fabrication of GO. In a typical experiment, graphite was utilized as a starting material, and GO was prepared using a modified form of the Hummers technique. A particular amount (98 mL) of sulfuric acid (H_2SO_4), 2 g of graphite, and 4g of $NaNO_3$ were taken in a 500 mL beaker and swirled for 2 h at low temperature ($T = 0−5$ °C). After that, 12 g of $KMnO_4$ was gradually added to it. The mixture was stirred continuously at 30−35 °C for approximately 2 h, and then the solution's temperature was raised to 90 °C for 10 min. After that, 200 mL of more water was added to the mixture and agitated for an hour. Then, 35 mL of 30% hydrogen peroxide was added, and the reaction mixture was stirred for 1 h. This resulted in change

Scheme 3. Schematic Representation for the Synthesis of Ag-Decorated Reduced Graphene Oxide (Ag-rGO)
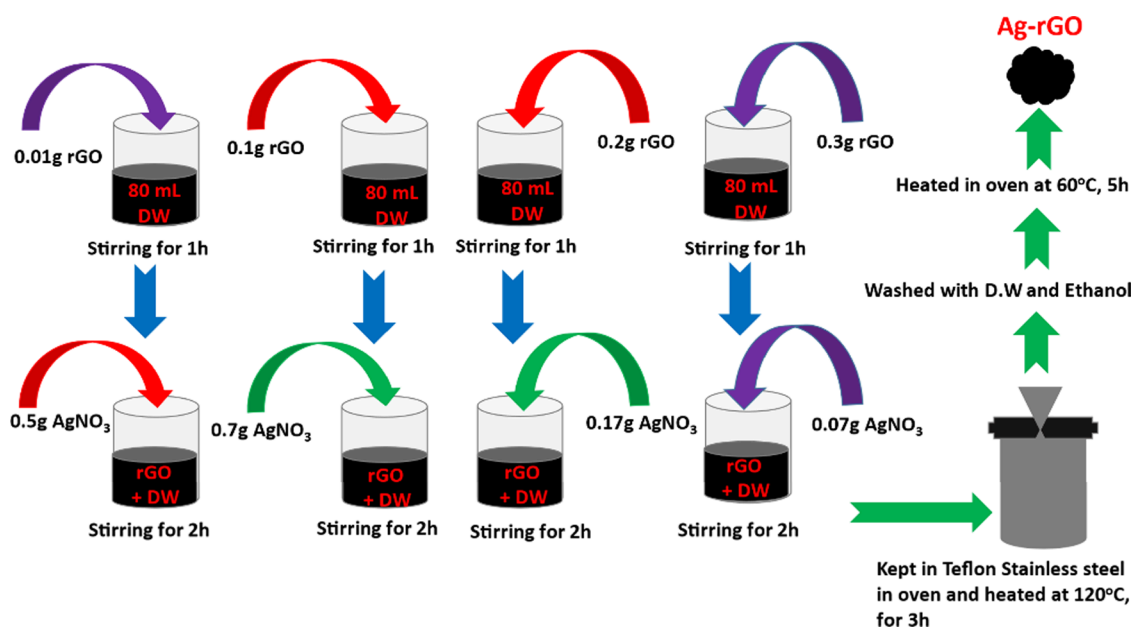
of solution's color from dark brown to a yellowish brown or yellowish color. The resulting mixture was kept at room temperature for approximately 15 h. Then, they were rinsed with ethanol and distilled water several times until the pH becomes neutral. After filtration and drying in oven at 60 °C for 10 h, the resultant material was named as GO.[53] The whole process is indicated in Scheme 1.

2.3. Fabrication of rGO. To prepare reduced graphene oxide (rGO), a hydrothermal method was employed. In a typical experiment, 1 g of graphene oxide (GO) was dispersed in 80 mL of distilled water to form a stable GO suspension. A few milliliters of ammonia solution was then added dropwise to adjust the pH of the suspension to 10. This solution was stirred for 24 h at room temperature and then transferred to a Teflon-lined autoclave. The autoclave, containing the reaction mixture, was placed in an oven at 180 °C for 24 h. Afterward, it was removed and allowed to cool naturally to room temperature. Following this, the solution was rinsed repeatedly with ethanol and distilled water to bring the pH to neutral. Finally, this solution was filtered and then dried in an oven at 70 °C for 8 h and later identified as rGO. A pictorial representation of the preparation of rGO is shown in Scheme 2.

2.4. Hydrothermal Preparation of Ag-rGO. To decorate reduced graphene oxide (rGO) with Ag, a hydrothermal approach was utilized. Initially, four beakers, each containing 80 mL of distilled water, were prepared. To these, different amounts of rGO, namely 0.01, 0.1, 0.2, and 0.3 g, were added to create homogeneous suspensions of rGO. All the suspensions were stirred for 1 h before adding 0.5, 0.7, 0.17, and 0.07 g of AgNO₃, followed by an additional 2 h of stirring. The mixture was then put into a Teflon-lined autoclave, sealed, and heated in an oven at 120 °C for 3 h. The mixture was subsequently washed multiple times with ethanol and distilled water to eliminate the residual nitrates. Finally, the mixture was filtered and dried in an oven at 60 °C for 5 h, resulting in the preparation of silver-decorated rGO, referred to as Ag-rGO. The schematic representation for the preparation of Ag-rGO is summarized in Scheme 3.

Various samples of Ag-rGO were prepared by varying the Ag-to-rGO ratio. All the materials, as mentioned in Table 1, were characterized by various techniques and employed as adsorbents and photocatalysts for Nile blue removal.

Table 1. Chemical Compositions of the GO, rGO, and Ag-rGO Samples Used in This Work Are Summarized

sample ID	chemical composition of constituents used	method used
Ag0.0-GO	graphite = 2 g; sodium nitrate = 4 g sulfuric Acid = 98 mL; KMnO₄ = 12 g H₂O₂ = 30 mL; H₂O = 200 mL	Hummers' method
Ag0.0-rGO	GO = 1 g; H₂O = 80 mL	hydrothermal
Ag0.5-rGO	rGO = 2 g AgNO₃ = 0.5 g; H₂O = 80 mL	hydrothermal
Ag0.7-rGO	rGO = 2 g AgNO₃ = 0.7 g; H₂O = 80 mL	hydrothermal
Ag0.17-rGO	rGO = 2 g AgNO₃ = 0.17 g; H₂O = 80 mL	hydrothermal
Ag0.07-rGO	rGO = 2 g AgNO₃ = 0.07g; H₂O = 80 mL	hydrothermal

2.5. Characterization of Materials. The structural, morphological, physicochemical, thermal, and textural features of the GO, rGO, and Ag-rGO nanomaterial samples were investigated via a variety of instruments, including the Lamda-25-PerkinElmer UV–visible spectrophotometer, R-Prestige-21-FTIR-8400S Shimadzu Fourier transform infrared spectrometer (FTIR), JSM-5910-JEOL scanning electron microscope, JEM-2100F transmission electron microscopic operated at 200 kV, energy-dispersive X-ray spectroscopy (EDX), and JEOL-JDX-3532 (JAPAN) X-ray diffraction (XRD) equipped with Cu Kα radiation source.

2.6. Adsorption Study on Removal of Nile Blue. Working solutions of various strengths (20, 40, 60, and 80 mg/L) were prepared from a 100 mg/L Nile blue stock solution for adsorption analysis. The fabricated materials (GO, rGO, and Ag-rGO) were used as adsorbents for the removal of Nile blue.[54] It was found that under the same experimental
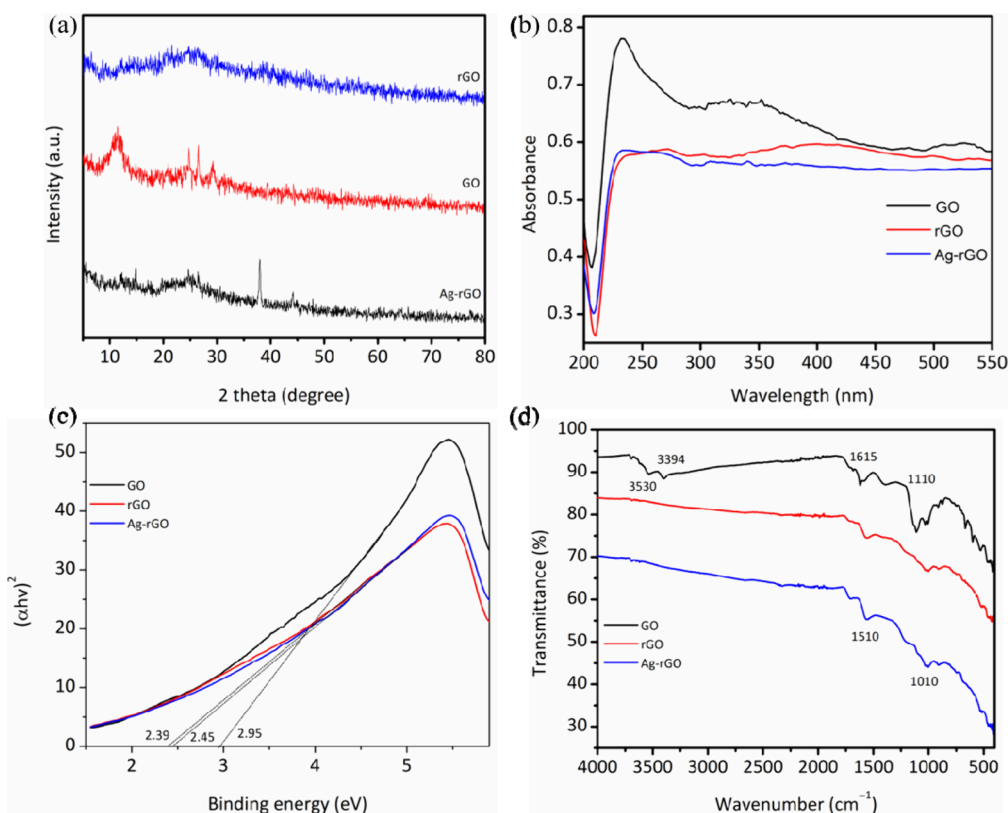
Figure 1. (a) XRD patterns, (b) UV−visible spectra, (c) Tauc plots for bandgap energy, and (d) FTIR spectra of GO, rGO, and Ag-rGO samples.

conditions, Ag-rGO exhibited the best performance. In a typical experiment, a specific amount of Ag-rGO (0.01 g) was added to 20 mL of dye solution, while using specific dye concentration, time, temperature, pH, and so forth. The solution was stirred for the desired time and filtered, and the filtrate was analyzed through UV−visible spectrometer to determine the equilibrium dye concentration after the adsorption of dye. A similar experiment was repeated under different experimental conditions. Adsorption capacity and dye adsorption % were determined using the following equations.[55]

$$\%\text{dye removal} = \frac{C_i - C_e}{C_i} \times 100 \tag{1}$$

$$q_e = \frac{C_i - C_e}{m} \times V \tag{2}$$

where q_e represents the adsorption capacity in mg/g, V represents the volume of NB dye solution in liters, C_i denotes the initial concentration of dye in mg/L, C_e stands for the concentration of dye in mg/L after filtration, and m means the adsorbent dose in gram.

2.6.1. Effect of Experimental Variables on the Adsorptive Removal of Nile Blue. To study the effect of experimental time on the adsorption of NB while using the mentioned adsorbents, seven bottles were employed. Each bottle contained a fixed concentration of dye (20 mg/L) solution and 0.01g/L of one of the adsorbents (GO, rGO, and Ag-rGO). The bottles, containing the dye-adsorbent, were stirred for different time intervals such as 10, 20, 30, 40, 50, 60, and 70 min followed by filtration. The filtrate of each bottle and for every adsorbent was then analyzed for the unadsorbed dye using a UV−visible spectrometer. For studying the effect of initial concentrations of dye, different solutions ranging from

10 to 50 mg/L were examined while other variables such as time = 60 min, pH = 6, temperature = 30 °C, and Ag-rGO dosage = 0.03g/L were kept constant. Likewise, the effect of adsorbent dose on the dye removal performance of the Ag-rGO was explored while maintaining other variables such as time = 60 min, pH = 6, temperature = 30 °C, and dye concentration = 20 mg/L constant. A typical experiment in this regard was carried out with a dosage of Ag-rGO ranging from 0.01 to 0.15 g per 20 mL of cationic dye solution (20 mg/L) while keeping other variables constant. Similarly, to investigate the effect of solution pH on the adsorption of NB, the adsorption experiments were conducted at different pH values while using 0.1 M HCl and 0.1 M NaOH to adjust the pH of the dye solution from acidic to basic medium while keeping other variables fixed; that is, time = 60 min, temperature = 30 °C, dye concentration = 20 mg/L, and the amount of Ag-rGO = 0.03 g/L. For this purpose, 12 beakers (20 mL) were used while each having dye + adsorbent at pH in the range of 1−12. In addition, the effect of temperature, in a temperature range of 303−353 K, on the percentage adsorption of NB over the surface of Ag-rGO was also studied. In this case, the parameters were used such as time = 60 min, pH = 6, dye concentration = 20 mg/L, and Ag-rGO = 0.03g/L. Additionally, an attempt was also made to investigate the impact of UV light (253 nm) on the removal of NB dye from water using Ag-rGO as an adsorbent at various time intervals, with all other parameters held constant.

2.6.2. Adsorption Equilibrium and Kinetics Studies. Adsorption results obtained by this method were examined using certain isotherm models so as to trace the physical properties of the interactions between NB dye molecules and Ag-rGO. The Freundlich model promotes surface heterogeneity due to variable adsorption energies, while the isotherm
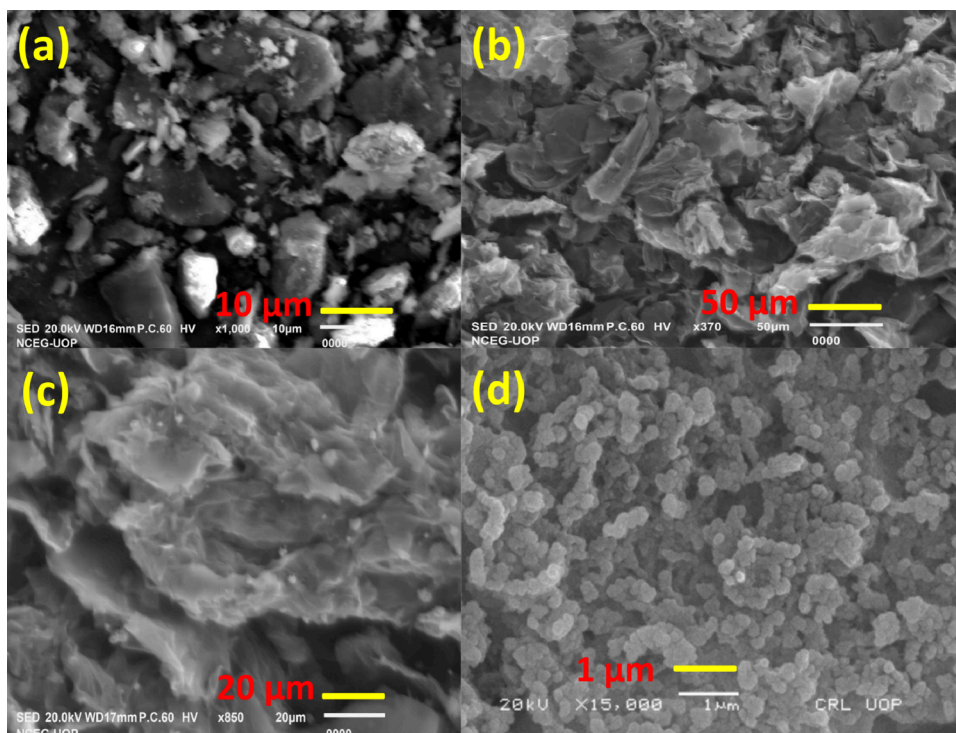
Figure 2. SEM images of (a) the GO, (b) the rGO, (c) the Ag-rGO, and (d) AgNPs.

of Langmuir is linked with surface featuring homogeneous adsorption sites that have comparable affinity to the adsorbate. Temkin isotherms assume that, once adsorbate/adsorbate interaction is considered, the heat of adsorption across all molecules that are in the layer decrease linearly with coverage.[56] This isotherm also underscores the adsorption process on the comparatively heterogeneous surface of the adsorbent

Kinetic studies, especially those involving the adsorption rate and adsorption equilibrium time, provide a great deal of information on the mechanism during adsorption tests. To investigate the NB adsorption kinetics on the Ag-rGO, two standard kinetic models, pseudo first-order and pseudo-second-order, were used. The latter implies that the process is regulated by an adsorption reaction at the adsorbent's liquid−solid interface, whereas the pseudo first-order process is regulated by diffusion and involves solid−liquid phase adsorption.

3. RESULTS AND DISCUSSION

3.1. Structural Morphology and Chemical Composition. The crystalline structure of the as-prepared GO, rGO, and Ag-rGO adsorbents was investigated by using XRD, and results are depicted in Figure 1a. The distinct diffraction peak at $2\theta = 11°$ appeared in GO sample but absent in rGO and Ag-rGO.[57] The XRD patterns of GO, rGO, and Ag-rGO catalysts indicate that GO exhibits a peak at $2\theta = 10°$, while in rGO, this peak shifted from $2\theta = 11°$ to $2\theta = 20°$, comparable to graphite; this result reveals that GO has been effectively reduced. Furthermore, the small peaks indicated in the GO may be due to the presence of graphite in a low quantity. Other possible impurities or structural defects in the GO sample may also account for these peaks. Such impurities or defects could induce additional crystalline phases and contribute to the broadening of the diffraction peaks. The

crystal structure of Ag-rGO has been identified, and the reduction of peak at $2\theta = 20°$ is due to the surface covered Ag NPs, which inhibited the stacking of rGO nanosheets.[58] According to the previous report,[59] the diffraction peak of GO at $2\theta = 11°$ corresponds to an interlayer spacing of 0.83 nm. The characteristic XRD peak of GO in Ag-rGO disappeared, and an additional broad peak appeared at $2\theta = 38°$. These variations also imply GO reduction.[60] The UV−visible absorption spectra of the samples are shown in Figure 1b. As expected, GO exhibits reflectance in the range of 230−280 nm, rGO possess reflectance in the range of 240−300 nm, and Ag-rGO displays reflectance in the range of 240−500 nm. In Ag-rGO, the smaller peak in the range of 400−500 nm is due to Ag, and its low intensity indicates that the content of Ag is low in the composite.

The bandgap energies of the GO, rGO, and Ag-rGO were also estimated through Tauc plot equation;[61] the results are presented in Figure 1c.

$$(\alpha h \upsilon)^\gamma = A(h\upsilon - E_g) \tag{3}$$

where α stands for the absorption coefficient, h stands for Plank's constant, υ denote the frequency of the photons, A represents the proportionality constant, E_g stands for the bandgap energy, and γ stands for the electron transition, which has the values of either 2, 1/2, 2/3, or 1/3, depending on transitions. For this purpose, $(\alpha h\upsilon)^2(\alpha h\upsilon)^2$ was plotted versus $(E = h\upsilon$ in units of eV). The extrapolated linear lines were used to estimate the bandgap, and the energy value was assigned to the point of intersection on X-axis. For GO, rGO, and Ag-rGO, the predicted bandgap energies are 2.95, 2.45, and 2.39 eV, respectively. As obvious, the bandgap energy values decrease while going from GO to rGO and then Ag-rGO. Similarly, 3.6, 1.5, and 2.4 eV,[62] 4.5 eV, 1.7, 3.7, and 1.4 eV,[63] have been reported by other scholars. The alteration in the bandgap values confirms the successful fabrication of the nanomaterials.
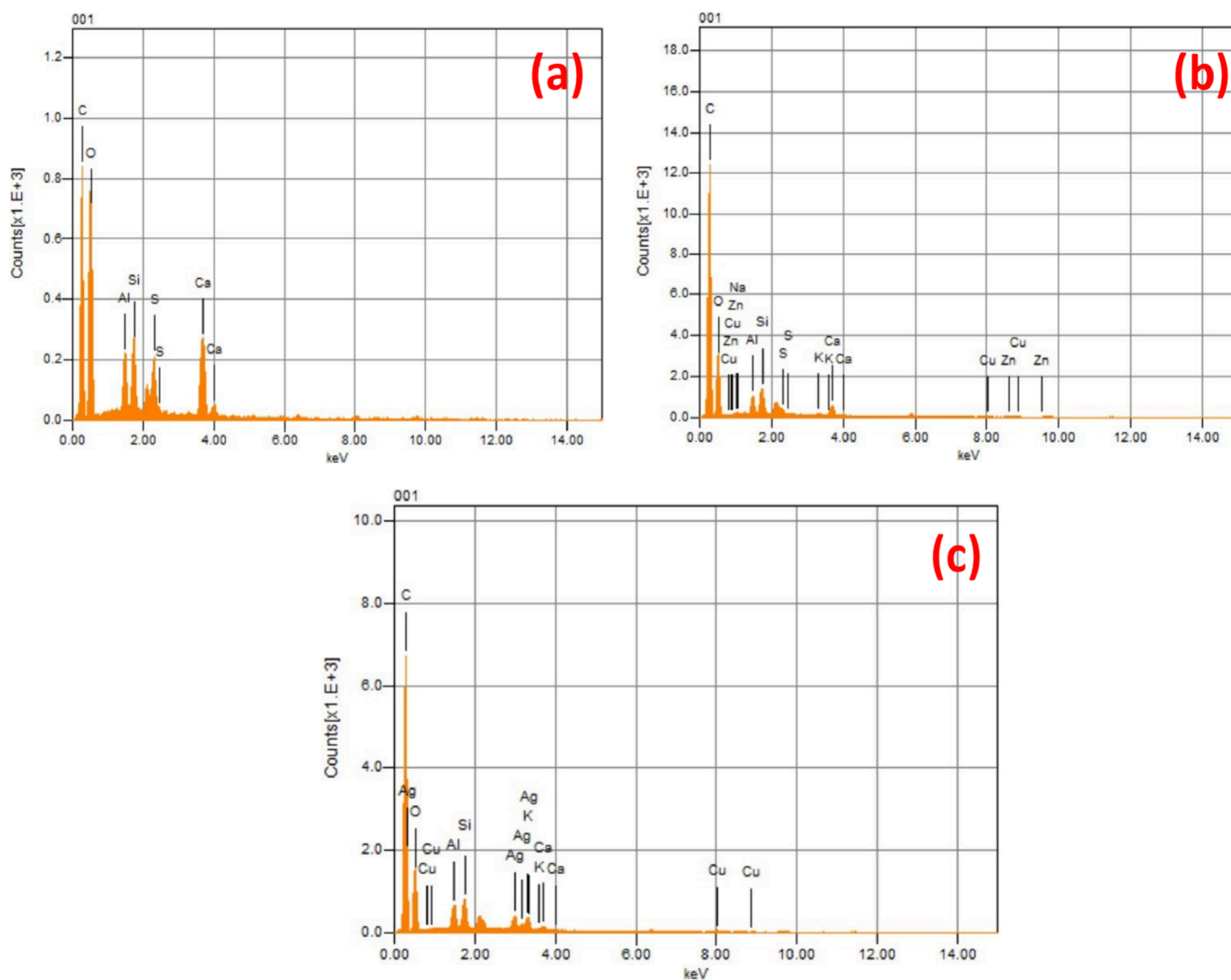
Figure 3. EDX analysis of (a) GO, (b) rGO, and (c) Ag-rGO.

This trend further supports the successful fabrication of catalysts. The differences in the bandgap values of GO, rGO, and Ag-rGO among themselves and with the reported materials may be due to the structural variations, environmental factors, doping or decoration, degree of reduction, the synthesis strategies and experimental conditions, and chemical composition of the synthesized nanomaterials.

The position and intensity of the FTIR peaks were used to get information about the possible functional groups and/or chemical composition of samples while analyzing the FTIR spectra in the range of 4000 to 400 cm^{-1}. The FTIR spectra of GO, rGO, and Ag-rGO are shown in Figure 1d. Some qualitative changes in the spectra indicate that GO is successfully transformed into rGO and, after decoration with Ag, Ag-rGO is formed. The disappearance of the prominent peaks of GO in the range of 3200−3400 cm^{-1} for rGO and Ag-rGO catalysts also reflects the successful transformation of GO to rGO in the as-fabricated catalysts. This trend is also supported by the qualitative changes in the position of other peaks of GO in the case of rGO and Ag-rGO. An additional peak at 423 cm^{-1} in Ag-rGO sample can be attributed to the Ag stretching transverse optical mode, which may be because of Ag^{2+} state, further endorsing the presence of Ag in the Ag-rGO nanocomposite.[10]

The microstructure and surface morphology of the adsorbents were estimated via the SEM analysis. The particle shape and morphology of GO appear asymmetric as indicated in Figure 2a, yet after reduction to rGO, distinct folds of flat sheets have been found shown in Figure 2b. The morphology and folded sheets of Ag-rGO are like those of rGO, except that spherical shaped Ag nanoparticles are evenly dispersed across the surface of rGO sheets, leading to a rougher surface.[58] This surface is well suited for the adsorption of hazardous organic contaminants such as dyes[1] indicated in Figure 2c. Finally, Figure 2d shows the sequential structure of virgin nanostructured Ag particles with some aggregation among them.

Figure 3 shows the energy-dispersive X-ray (EDX) spectra of the nanomaterials. As expected, primary peaks related to carbon, sulfur, oxygen, zinc, aluminum, copper, silicon, calcium, and silver have been found.[64] In the case of the Ag-rGO adsorbent, the atomic weight percentage of oxygen, carbon, and silver elements are found to be 49, 39, and 3.19%, respectively. This proves the successful fabrication of the Ag-rGO composite. Furthermore, the presence of impurities in the rGO was noted, which may originate from possible contaminants in the sample holder during analysis, along with some minor impurities in the materials used during the synthesis. The EDX analysis also revealed a decrease in oxygen

content and a corresponding increase in carbon content from GO to rGO. The conversion of GO to rGO is further confirmed by the change in the morphology observed in the SEM analysis.

3.2. Adsorption Study. *3.2.1. Effect Time Period and Chemical Nature of the Materials on NB Dye Removal.* The three types of materials such as GO, rGO, and Ag-rGO were tested for their adsorptive performance toward the removal of Nile blue dye at different time intervals in the range of 10−70 min with a 10 min interval while keeping all other experimental variables fixed. Equations 1 and 2were used to calculate the % adsorption and adsorption performance (mg/g) for each adsorbent at each interval of times. The results indicated that equilibrium was reached after 50 min for a 20 mg/L dye solution containing 0.01g/L of Ag-rGO, rGO, and GO in a 20 mL solution. According to these findings, the percent adsorption capacity of all adsorbents for NB removal is most prominent within the first 10−50 min and remains nearly constant thereafter. The initial rate of dye uptake by Ag-rGO nanoparticles improves dramatically over time, reaching a maximum (94%) after 60 min. This means that the molecules of the dye could establish a layer on the outer surface of the adsorbents. This is corroborated by the fact that the adsorption rate of dye over the composite is primarily regulated by mass transfer.[65] It is observed that at 50 and 60 min, the NB removal rates are 93.8 and 94% with adsorption capacities of 37.5 and 37.6 mg/g for Ag-rGO-based adsorbent. Since there is no substantial increase in % adsorption and adsorption capacity after 60 min, this time is considered the equilibrium and optimum time for further experiments. Likewise, during this time period, about 49−50% of NB was adsorbed over the rGO and 22% over the surface of GO as revealed in Figure 4. Based
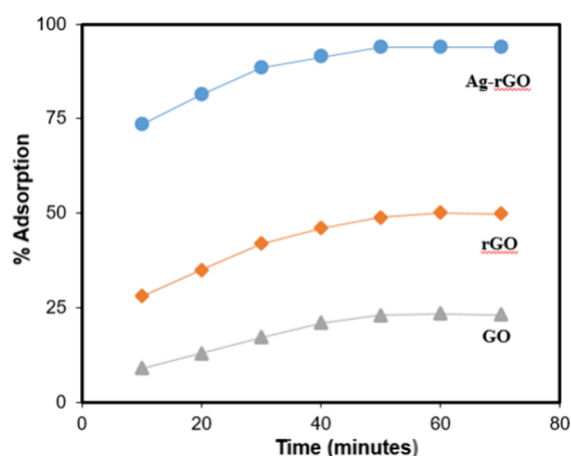
Figure 4. Effect of time on the % adsorption of NB at the surfaces of GO, rGO, and Ag-rGO at T = 30 °C, pH = 6, adsorbent amount = 0.01g/L, dye concentration = 20 mg/L, and volume = 20 mL.

on these findings, it is evident that Ag-rGO-based adsorbent exhibits the best adsorption capacity toward NB dye removal. Therefore, the performance of this adsorbent was studied in detail by maintaining the experimental time at 60 min and varying other variables such as the amount of adsorbent, initial concentration of NB, solution pH, and temperature.

3.2.2. Effect of Experimental Variables on the Removal of NB Dye using Ag-rGO. Figure 4 reveals that Ag-rGO has the best adsorption capacity toward the NB dye. Thus, the effect of various experimental variables such as dye concentration,

amount of adsorbent, solution pH, and temperature on the % removal of NB dye was investigated in detail, and the results are shown in Figure 5.

3.2.2.1. Effect of Initial Concentrations of NB. The effect of initial dye concentrations, as indicated in Figure 5a and ranging from 10 to 50 mg/L, was examined while all other variables were kept constant. It can be seen that as the dye concentration increases, the percentage of NB adsorption decreases, while the dye adsorption capacity (mg/g) increases. It is expected that the reduction in adsorption is caused by repulsion among the adsorbed dye and adsorbate molecules in the bulk medium or by a decrease in the availability of vacant sites over the surface of the adsorbent.[66] The highest NB adsorption capacity (mg/g) was achieved at 50 mg/L of the original dye concentration, but minimal % adsorption was also observed at the same dye concentration. It was found that under these conditions, about 90% of NB could be removed, demonstrating that Ag-rGO is an efficient adsorbent for dye removal from aqueous media. It can also be said that the Ag-rGO-based adsorbent is equally efficient in both dilute and concentrated dye solutions.

3.2.2.2. Effect of Adsorbent Dose. Similarly, the effect of the adsorbent dose on the dye removal performance of the Ag-rGO was explored while maintaining other variables constant, as depicted in Figure 5b. The studies involved varying the dosage of Ag-rGO from 0.01 to 0.15 g per 20 mL of cationic dye solution (20 mg/L). The adsorption percentage increases to a particular level (0.03 g/L) and then drops as the dosage of adsorbent increases. It is possibly due to an increase in the number of exposed adsorption sites on the surface of the material that could grab the dye molecules, thereby favoring the adsorption process.[29] Furthermore, introducing more nanoadsorbents to the solution medium after a specific amount of adsorbent reduces NB dye removal by adsorption. Furthermore, the increasing availability of nanoscale adsorbents might have an adverse effect on the ·OH radical removing action. Consequently, it may lead to a decrease in removal of dye from a solution medium by adsorbent.[53]

3.2.2.3. Effect of Solution pH. It is also observed that wastewater containing dyes is released at different pH levels, making it essential to investigate NB dye removal under different pH conditions. Experiments were conducted at different pH values while using 0.1 M HCl and 0.1 M NaOH to adjust the pH of the dye solution from an acidic to a basic medium while keeping other variables fixed. The results depicted that the % adsorption of NB is increased with pH from acidic to pH = 6 and then decreased with further increase in the solution pH as shown in Figure 5c. So, it shows that pH affects the surface charge of the adsorbent particle directly or indirectly. Furthermore, pH also impacts the ionization behavior of the dye, leading to fluctuations in the interaction of dye molecules with the adsorbent surface; as a result of these changes, variations in the pH of the solution can impact the adsorption process. The approximate pK_a value for Nile Blue dye is 6−6.2. It reflects that at pH < 6 (acidic environment), NB exists in its protonated form (cationic), whereas at a pH > 6, it exists primarily in its deprotonated form (neutral). In an acidic environment (low pH), NB dye molecules have been observed to be protonated. Under these conditions, it has less opportunity for attaching to a surface with a positive charge due to the possible electrostatic repulsion between NB and adsorbent surface. In addition, the proton ions for the NB dye and adsorption sites are also competing. The interaction
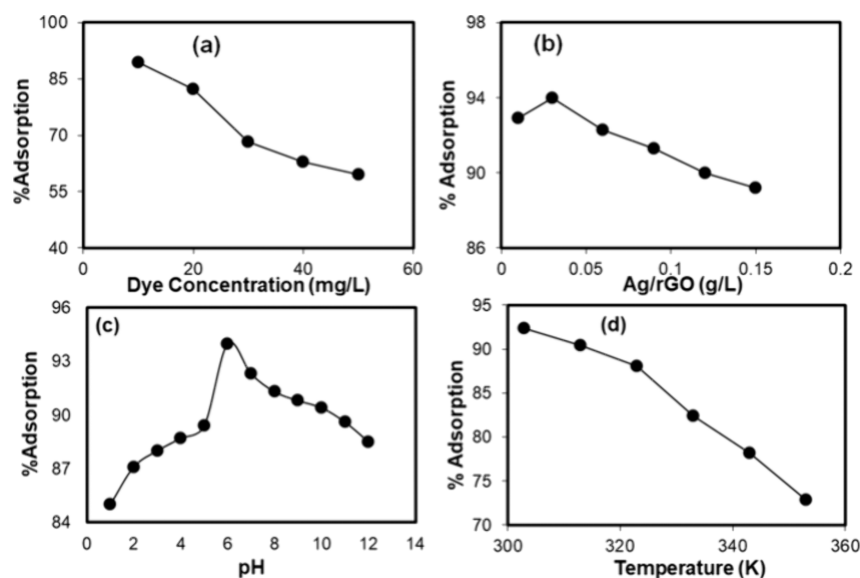
Figure 5. Effect of (a) dye concentration, (b) adsorbent dose, (c) pH of the medium, and (d) temperature on the % adsorption of NB using Ag-rGO as an adsorbent at time = 60 min.

between the more significant binding site of the complex surfaces and the functional group of dye increases the % adsorption capacity of Ag-rGO with pH up to neutral. While at neutral pH, NB is expected to be almost neutral; hence, it can attach better to any surface fruitfully; thus, adsorption is maximum in the pH range of 6−7 in the current studies. Similarly, increasing the pH above neutral conditions decreases the concentration of hydrogen ions (H^+) in solution, and the NB molecules start to lose their positive charge and become more negatively charged. Consequently, it becomes more challenging for these negatively charged molecules to adhere to negatively charged surfaces, leading to decreased adsorption under alkaline pH conditions. These fluctuations arise due to the electrostatic interactions between the negatively charged surface sites of Ag-rGO and NB dye. When the pH of the solution exceeds pH 7, the electrostatic repulsion between negatively charged surfaces and negatively charged dye molecules increases, resulting in a decreased adsorption rate.[66] Under an acidic environment (low pH), the surface of Ag-rGO is likewise expected to be protonated, resulting in a net positive charge. Under these conditions, it is anticipated that different surface groups, including carboxyl, hydroxyl, and epoxide groups, will lose their negative charge, resulting in a positively charged surface overall. Similarly, at higher pH (alkaline environment), the surface is projected to be negatively charged due to surface functional group deprotonation. All of these changes in the surface chemistry of Ag-rGO and NB dye molecules resulting from changes in solution pH significantly influence the adsorption process. While studying the effect of solution pH on adsorption efficiency of the adsorbent, the information regarding the point of zero charge (pH_{pzc}) of the adsorbent is essential. The pH_{pzc} of the adsorbent is the pH at which the surface of a material has no net electrical charge. This value significantly impacts the adsorption of adsorbate molecules on the adsorbent's surface. Therefore, the pH_{pzc} values of the materials were also determined through the pH drift method. To do this, first different buffer solutions ranging from acidic to alkaline pH and then the adsorbent samples were submerged in each pH buffer overnight to allow the material's surface charge to adjust

to the solution pH. The pH−surface charge curves were made by plotting the experimental pH values on Y-axis and the theoretical pH values on X-axis indicated in Figure 6. The
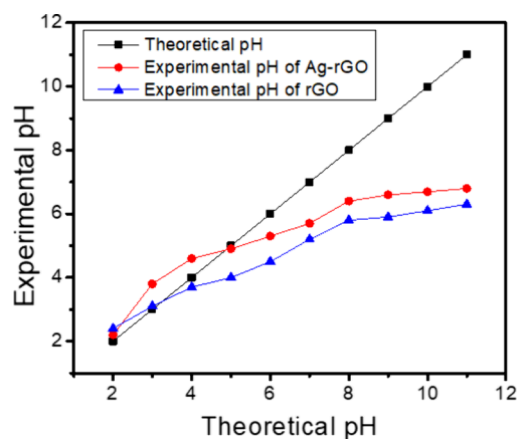
Figure 6. Assessment of point of zero charge (pH_{pzc}) for rGO and Ag-rGO.

point of zero charge (PZC) for the adsorbents was determined as the point where experimental pH values intersected theoretical pH values in plots. The pH_{pzc} of GO and rGO was found in the range of 2.5−3.5, while that of Ag decorated rGO was found to be 5.2. It means that the introduction of Ag nanoparticles shifts the pH_{pzc} closer to neutral. The surface of the material is expected to be negatively charged at pH levels above the corresponding pH_{pzc} and would be suitable for the adsorption of positively charged dye molecules. On the contrary, when the solution pH is below the pH_{pzc}, the adsorbent's surface becomes positively charged, and it would not be suitable for adsorbing positively charged dye molecules. Based on the pK_a value of NB and pH_{pzc} of Ag-rGO, it is suggested that pH of solution prominently affects the adsorptive removal of NB through Ag-rGO.

3.2.2.4. Effect of Experimental Temperature. Similarly, the effect of temperature on the percentage adsorption of NB over the surface of Ag-rGO was studied in a temperature range of
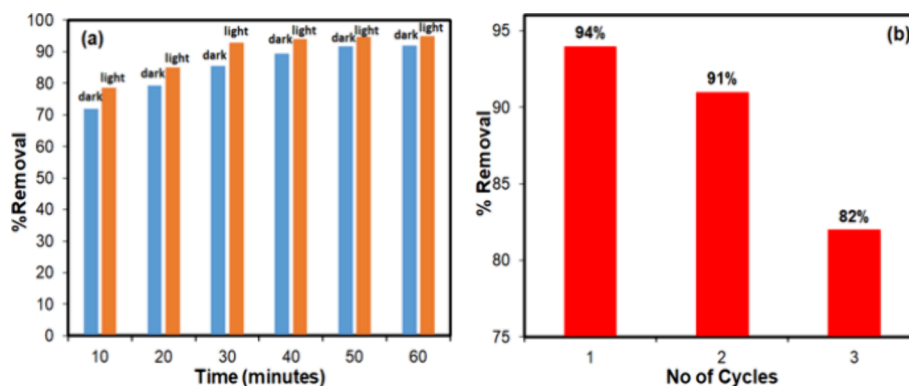
Figure 7. Comparison of % removal of NB dye through Ag-rGO, in the absence and presence of (a) light and (b) recycling performance of Ag-rGO toward the removal of NB dye from water at different intervals of time and at time = 60 min, T = 30 °C, pH = 6, adsorbent amount = 0.03g/L, and dye concentration = 20 mg/L.

303−353 K, and the results obtained are provided in Figure 5d. As obvious, the adsorption process decreases with increasing temperature, indicating that the entire process is exothermic. As the temperature rises, the rate of NB adsorption decreases from 92.4 to 72.9%. This decrease can be attributed to the solubility of NB in bulk water, which is temperature-dependent. At higher temperatures, dye molecules are more likely to stay in the solution rather than migrate to the solid surface of Ag-rGO. In other words, the interaction forces between the NB solute and the water (solvent) molecules become stronger than the interactions between the NB solute and solid Ag-rGO. Consequently, loading the NB solute onto the active sites of Ag-rGO becomes more challenging. As a result, Ag-rGO seems to be a more effective adsorbent for adsorbing NB at lower temperatures.[67]

3.2.3. Effect of the Presence of Light on the Removal of NB Dye. An attempt was also made in this work to see the effect of light (UV, 253 nm light source, SonyoDengy Japan) on the removal of NB dye from water using Ag-rGO as an absorbent at different time intervals while keeping all other parameters constant. The test for photoassisted removal of NB experiment of NB was performed at different time intervals (10−60 min) while maintaining other parameters constant: pH = 6, temperature = 30 °C, dye concentration = 20 mg/L, and the amount of Ag-rGO was 0.03 g/L. A similar experiment was carried out in the absence of light, and the outcomes of both photoassisted removal of Nile blue (NB) and adsorptive removal (in the absence of UV-light) are compared, as shown in Figure 7a. In each experiment, 10 mL of solution was extracted from both reacting solutions after every 10 min interval of time, and the remaining concentration of dye in the filtrate was evaluated using a UV−visible spectrophotometer, and the percent removal was estimated using eq 1. The percentage removal of dye by Ag-rGO in the presence and absence of light was plotted vs time as indicated in Figure 7a. It can be observed that, after 60 min of the reaction and under the same conditions, 95% of NB dye is removed in the photoassisted experiment, while 92% of NB is adsorbed by Ag-rGO. This difference indicates that the presence of light has enhanced the adsorptive removal of NB dye while using Ag-rGO as an adsorbent.

The possible photocatalytic mechanism for the photo-assisted removal of NB over Ag-rGO is summarized in Scheme 4. When light with energy greater than the bandgap of the semiconductor (rGO) is absorbed by the material, it results in

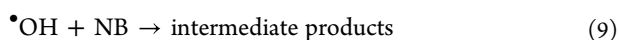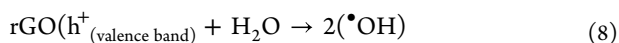**Scheme 4. Schematic Representation for the Photoassisted Removal of NB over the Ag-rGO**
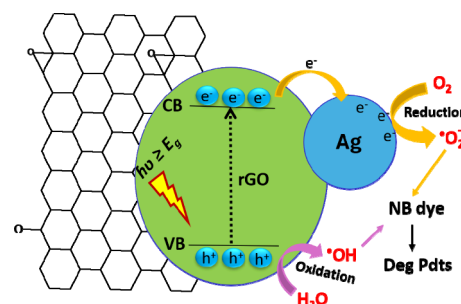
the promotion of electrons from the valence band (VB) to the conduction band (CB) and creation of electron−hole pairs (e^- (conduction band) + h^+ (valence band)). These created species migrate along their respective pathways within the semiconductor, thereby avoiding the recombination of electron−hole pairs. This is attributed to the efficient charge transfer facilitated by the built-in electric field at the Ag-rGO interface. The migration of excited electrons, located in the conduction band (CB) of rGO, to Ag takes place due to the formation of a Schottky barrier between rGO and Ag in the nanocomposite. At the Ag-rGO interface, due to the lower work function of Ag compared to rGO, electrons tend to accumulate at the Ag surface, while holes remain within the rGO. Electrons trapped at the Ag-rGO interface can facilitate the reduction of adsorbed species, such as oxygen molecules (O_2), resulting in the generation of reactive oxygen species (ROS) like superoxide radicals ($^{\cdot}O_2^{2-}$). These ROS then participate in degradation of pollutant (NB) and transform it into intermediate products and finally into CO_2, H_2O. Similarly, the holes in the rGO can oxidize adsorbed species, such as water (H_2O), into hydroxyl radicals ($\cdot OH$), which in turn degrade the pollutant (NB) into intermediate products and finally into CO_2, H_2O. Summary of the possible reactions during this photoassisted NB removal over the surface of Ag-rGO are given below.

$$Ag - rGO + h\nu \rightarrow Ag$$
$$- rGO(h^+_{(valence\ band)} + e^-_{(conduction\ band)})$$
$$(4)$$
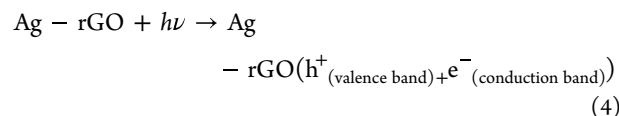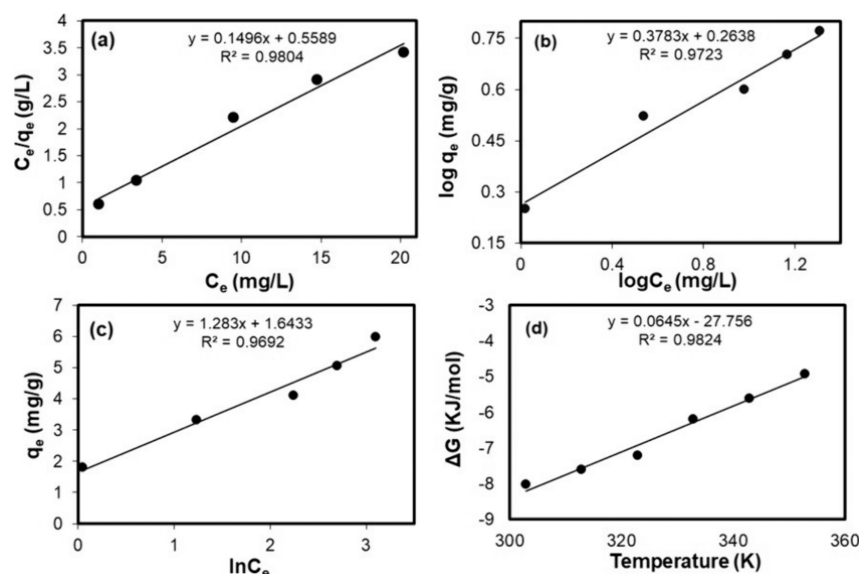
Figure 8. Representation of the linear fitting version of adsorption isotherms, (a) Langmuir, (b) Freundlich, (c) Temkin, and (d) the variation in the values of Gibbs free energy changes (ΔG) as a function of temperature for the adsorption of NB using Ag-rGO as an adsorbent at time = 60 min, T = 30 °C, pH = 6, adsorbent amount = 0.03g/L, and dye concentration = 20 mg/L.

$$Ag - rGO(h^+_{(valence\ band)} + e^-_{(conduction\ band)})$$
$$\rightarrow Ag(e^-) + rGO(h^+) \tag{5}$$

$$Ag(e^-_{(conduction\ band)}) + O_2 \rightarrow {}^\bullet O_2^- \tag{6}$$

$${}^\bullet O_2^- + NB \rightarrow intermediate\ products \tag{7}$$

$$rGO(h^+_{(valence\ band)}) + H_2O \rightarrow 2({}^\bullet OH) \tag{8}$$

$${}^\bullet OH + NB \rightarrow intermediate\ products \tag{9}$$
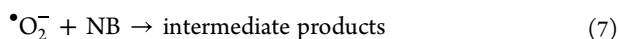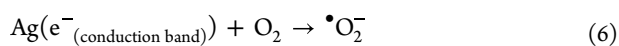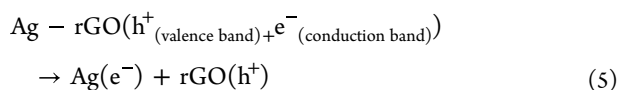
3.2.4. Reusability Performance of Ag-rGO. The recycling stability test of the Ag-rGO nanocomposite toward the removal of NB dye from an aqueous medium was conducted over three consecutive cycles under consistent experimental conditions: time = 60 min, temperature = 30 °C, initial NB concentration = 20 mg/L, pH = 6, and adsorbent amount = 0.03 g/L. After the first cycle of the experiment, the adsorbent material (Ag-rGO) was recovered, washed with water, and dried in an oven at 100 °C for an hour before being reused in the subsequent cycle for dye removal. As depicted in Figure 7b, the percentage of dye removed was calculated and presented as a function of the number of cycles. The results indicate that 94% of NB was removed in the first cycle, 91% in the second cycle, and 82% in the third cycle. The observed decrease in the dye removal performance of Ag-rGO in successive cycles could be attributed to a slight loss in the adsorbent amount and minor alterations to the active sites on the material surface. In general, the overall recycling performance was satisfactory, revealing that Ag-rGO performed well in terms of NB removal from water under the experimental conditions utilized here.

To further understand the better reusability, recycling ability of the adsorbent, and stability of the Ag-rGO composite (Ag-rGO), the Ag leaching experiments, which involve studying the release of silver ions (Ag⁺) into a solution, were also performed. All such measurements were carried out in aqueous solutions at various pH conditions, including acidic, neutral, and alkaline pH. In a typical experiment, 0.5 g/50 mL of Ag-rGO was dispersed in the leaching solution to create a

suspension, ensuring thorough mixing to promote interaction between Ag-rGO and the solution. The mixture was stirred for approximately 4 h at room temperature. An aliquot amount (5 mL) of the dispersion was collected at 30 min intervals, followed by centrifugation. The remaining filtrates were then analyzed using a UV−visible spectrometer; however, no peak was observed in the 400 to 500 nm range. Typically, the λ_{max} for silver ions in water is observed in this range of the UV−visible spectrum. These results indicate the absence of noticeable Ag leaching. In other words, the findings offer insights into the stability of the Ag-rGO composite under the experimental conditions used in this study.

3.3. Adsorption Isotherm. *3.3.1. Langmuir isotherm.* The application of the Langmuir adsorption isotherm to equilibrium adsorption was made possible by assuming the existence of monolayer adsorption over the adsorbent having a small number of identical sites. The Langmuir isotherm linear formula is shown below:

$$\frac{C_e}{q_e} = \frac{C_e}{q_m} + \frac{1}{q_m K_L} \tag{10}$$

In eq 10, the terms C_e, q_e, q_m, and K_L denote the NB dye equilibrium concentration, equilibrium adsorption capacity, maximum adsorption capacity, and Langmuir constant, respectively. The linear plot of C_e/q_e vs C_e shown in Figure 8a provides q_m (mg/g) and K_L (L/mg), indicating the efficacy of adsorbate−adsorbent interactions. In other words, K_L is related to the affinities of binding sites, as well as the free energy of adsorption. The term q_m (mg/g) tells us about the quantity of dye that is present whenever a single layer forms on the adsorbent. The values for q_m and K_L were predicted using the slope and intercepts of the C_e/q_e versus C_e plot, respectively.[56]

3.3.2. Freundlich Isotherm. The Freundlich model illustrates the reversibility of adsorption, highlighting its physical characteristics and potential for multilayer development on relatively heterogeneous surfaces. This model also suggests that adsorbent surfaces exhibit diversity in nature and

are particularly suitable for systems with heterogeneous surface energy. Equation 11 shows the linear form of the Freundlich isotherm.[56]

$$\log q_e = \log K_F + \frac{1}{n} \log C_e \tag{11}$$

where "q_e" refers to the quantity of dye adsorbed per unit weight of adsorbent, "C_e" represents the equilibrium concentration of dye within the bulk solution, "K_F" refers to the Freundlich constant that reveals the adsorbent's relative adsorption capacity (mg/g), and "n" (g/L) indicates adsorption intensity within the Freundlich equation and corresponds to the interaction among the adsorbate and adsorbent.[68] A typical Freundlich plot ($\log q_e$ versus $\log C_e$) is revealed in Figure 8b.

3.3.3. Temkin Adsorption Isotherm. It also emphasizes adsorption on the somewhat heterogeneous surface of the adsorbent. This model operates on two major assumptions: (i) it provides details regarding the adsorbate/adsorbent interactions and the enthalpy of adsorption, asserting that the heat of adsorption rises as the surface is covered and (ii) it posits adsorption as a uniform dispersion of binding sites with uniform energies up to a certain limit.[69] The linear form of its typical equation is as follows:

$$q_e = B \ln K_{TM} + B \ln C_e \tag{12}$$

where K_{Tm} and B represents the Temkin's adsorption constants, with K_{Tm} corresponds to the maximum binding energy (mg/L), and B refers to the heat of adsorption. The slope and intercept of the linear plots of q_e vs $\ln C_e$ indicated in Figure 8c were used to determine these values.

The data related to the adsorption of NB at the surface of Ag-rGO were tested through Freundlich, Temkin, and Langmuir isotherms, and the results are provided in Figure 8a–c and Table 2. The results indicate that all the data can be

Table 2. Summary of the Calculated Parameters of Different Adsorption Isotherm Models for Adsorption of NB Dye on Ag-rGO

adsorption isotherm models	parameters	Ag-rGO (adsorbent)
Langmuir	q_m (mg/g)	6.685
	K_L (L/mg)	0.267
	R^2	0.980
Freundlich	n	2.643
	K_F (mg/g)	1.835
	R^2	0.972
Temkin	B (j/mol)	1.283
	K_{KT} (L/mg)	3.599
	R^2	0.9692

fitted to all these models; however, based on values of regression constant (R^2), the fitting order follows the sequence, Langmuir > Freundlich > Temkin model. According to the results of the Langmuir isotherm, the adsorptive removal of NB dye through Ag-rGO-based adsorbent is of monolayer type at the homogeneous adsorbent surface via chemisorption process.[1] Based on the results of various models, it is also proposed that the adsorption process is not merely chemical or physical in nature; rather, it is deemed to be of a physicochemical nature. It is assumed that there are physicochemical interactions, such as van der Waals forces, hydrogen bonding, and electrostatic attraction, between the

surface of the Ag-rGO catalyst and NB dye molecules. It also implies that the material's surface is not completely homogeneous, owing to the heterogeneous nature of the active sites found on the surface of Ag-rGO. Furthermore, the adsorption data was subjected to analysis using nonlinear isotherm equations, such as Langmuir, Freundlich, and Temkin isotherms, represented by plots of q_e versus C_e (Figure 9a–c). Both linear and nonlinear plots of the isotherm models were found to be satisfactory. However, linear plots offer greater simplicity and ease for new readers to evaluate the suitability of the data to the respective equations, compared to their nonlinear counterparts.

3.4. Kinetics Study of Adsorptive Removal of NB Dye. In order to get some insight about the adsorption mechanism, the data were tested through pseudo first-order and pseudo second-order kinetics models. The linear form of the model is as follows:

The linear form of pseudo first-order model equation is as follow.[70]

$$\log(q_e - q_t) = \log q_e - \frac{k_1 t}{2.303} \tag{13}$$

Here, q_e and q_t denote amounts of the NB bound on prior to achieving equilibrium, whereas t denotes time and k_1 is the reaction rate constant. The slope of the graph of the changing $\log(q_e - q_t)$ was used to determine the constant for the reaction rate (k_1) values. The pseudo-second order equation was also used to determine how the NB adsorption on various adsorbents react chemically. The pseudo second-order model is given as

$$\frac{t}{q_t} = \frac{1}{k_2 q_e^2} + \frac{t}{q_e} \tag{14}$$

Similarly, k_2 and q_e values can be obtained from the slopes and intercepts of plots of (t/q_t) versus time (t), respectively. The graphs of pseudo-first- and pseudo-second-order kinetic models are presented in Figure 10a,b, respectively. Table 3 provides a summary of all of the important parameters derived from these kinetic models. The results supported the notion that the adsorption process is physicochemical in nature, as the calculated q_e values from both models (first and second order) closely match the experimental values, and the correlation factor (R^2) values are also in good agreement. However, the regression factor (R^2) result for the pseudo-second-order reaction is higher ($R^2 > 0.99$), indicating that the kinetic data best conforms to this model. Accordingly, the chemisorption contribution to the current adsorption process is deemed significant.[70]

The adsorption kinetics were also assessed through a linear intraparticle diffusion model eq 15.

$$q_t = K_{diffusion} \times t^{1/2} + C \tag{15}$$

The diffusion coefficient or the quantity of a substance expected to diffuse into the medium at a given time in the future can be estimated by using the equation describing the diffusion of a substance into a medium. "q_t" tells that how much adsorbent/material can be diffused into the medium in time "t". It addresses the aggregate mass or volume of diffuse material that enters the medium up to that point. K_{diff} is the diffusion coefficient or diffusivity of the diffusing adsorbent, indicating how easily a substance diffuses through a medium. It is influenced by the medium's properties, molecular size, and
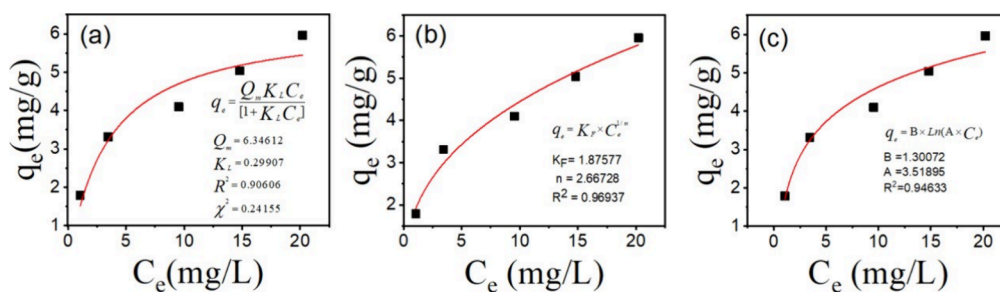
Figure 9. Representation of the nonlinear fitting version of adsorption isotherms, Langmuir (a), Freundlich (b), and Temkin (c) models for the adsorption of NB using Ag-rGO as adsorbent at Time = 60 min, T = 30 °C, pH = 6, Adsorbent amount = 0.03g/L, and Dye concentration = 20 mg/L.
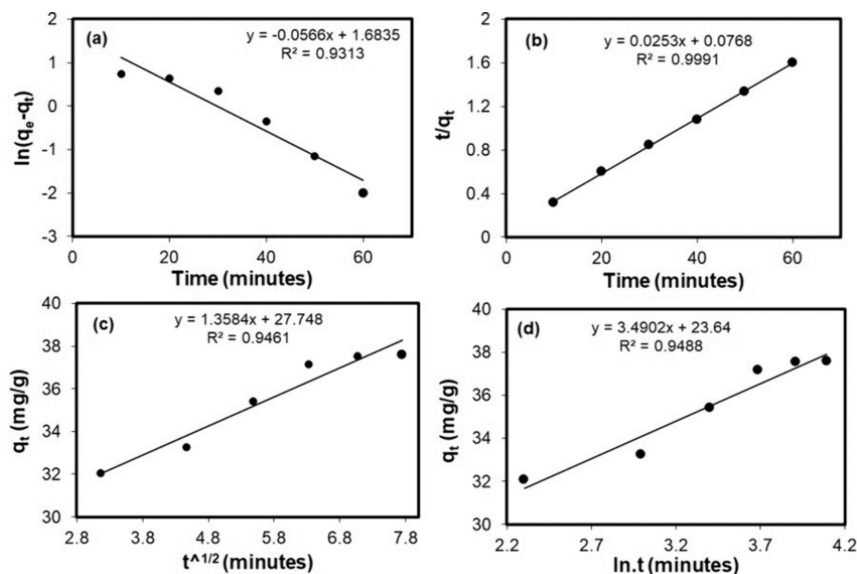
Figure 10. Representative adsorption kinetics plots, (a) pseudo-first order, (b) pseudo-second order, (c) the intraparticle diffusion model, and (d) the linear Elovich kinetics model for the adsorption of NB using Ag-rGO as an adsorbent at time = 0−60 min, T = 30 °C, pH = 6, adsorbent amount = 0.03g/L, and dye concentration = 20 mg/L.

Table 3. Summary of the Kinetics Parameters of Pseudo-First Order, Pseudo-Second Order, Elovich, and Intraparticle Diffusion Model for Adsorption of NB Dye on Ag-rGO

adsorption kinetics models	parameters	values
pseudo-first order	calculated q_e (mg/g)	48.250
	k_1 (min^{-1})	0.056
	R^2	0.931
pseudo-second order	calculated q_e (mg/g)	39.52
	k_2 (g/mg.min)	0.004
	R^2	0.999
intraparticle diffusion model	calculated q_t (mg/g) at t ≈ 0	27.74
	$K_{diffusion}$ (mg/g.min)	1.3584
	R^2	0.946
Elovich kinetics model	β (mg/g.min)	3054.89
	α (g/mg)	0.286
	R^2	0.948

shape of the adsorbate, medium, and adsorbent and some other experimental variables. In the present case, the unit of K_{diff} is mg/g·minute. Similarly, "C" is the intercept of the plot, which represents the amount of material that has already diffused into the medium at time zero. It is also referred to as the initial condition or boundary condition of the adsorption

process. All of these parameters were estimated from Figure 10c and are given in Table 3. The correlation factor (R^2) values obtained from this model are also in good agreement. This indicates that the diffusion process is also playing role in the dye removal process. Since pseudo-second order kinetics exhibit a higher R^2 value than pseudo-first order and intraparticle diffusion kinetics models, the chemisorption contribution in adsorptive removal of NB through Ag-rGO-based adsorbents cannot be overlooked. It is concluded that this adsorption process is of a physicochemical nature with a substantial contribution from a diffusion-controlled phenomenon as well.

Likewise, the adsorption data were also tested with the Elovich kinetic model. It is also an informative model because it describes the chemisorptive feature of dye/adsorbate adsorption on solid surfaces in general. The simplified versions of Elovich kinetics model are presented in eqs 16 and 17.[71]

$$q_t = \frac{1}{\beta}\ln(\alpha\beta t + 1) \text{ nonlinear} \tag{16}$$

$$q_t = \frac{1}{\beta}\ln(\alpha\beta) + \frac{1}{\beta}\ln t \text{ linear} \tag{17}$$

In these equations, the terms β, α, and q_t reflect the adsorption rate (mg/g·min), the desorption constant (g/mg),

Table 4. Thermodynamics Parameter for the Adsorption/Removal of Nile Blue on the Surface of Ag-rGO

temperature (K)	q_e(mg/g)	C_e(mg/L)	values of $K_{eq}(K_e = q_e/C_e)$	values of $[\ln(q_e/C_e)]$	ΔG(kJ/mol)	ΔH(kJ/mol)	ΔS(kJ/mol)
303	36.96	1.52	24.31	3.19	−8.04		
313	36.96	1.92	18.83	2.93	−7.62		
323	35.24	2.38	14.81	2.69	−7.22	−27.76	+0.0645
333	32.96	3.52	9.36	2.24	−6.20		
343	31.30	4.35	7.19	1.97	−5.62		
353	29.16	5.42	5.38	1.68	−4.93		

and the quantity adsorbed at time "t" in mg/g. The data was evaluated using the Elovich adsorption model's linear and nonlinear equations. A user-defined equation $(q_t = 1/B \times (\ln(A \times B \times t + 1)))$ was used for the nonlinear model, where A and B indicate α and β, respectively. In the case of the linear model, the data was fit directly in the origin using eq 18, and the results are shown in Figure 10d.

3.5. Thermodynamics Investigations.
Equations 18−20 were employed to calculate the relevant thermodynamic parameters using the adsorption data at various experimental temperatures. The equilibrium constant (K_{eq}), change in Gibbs free energy (ΔG), enthalpy change (ΔH), and entropy change (ΔS) are among these parameters. These measurements can provide information on the energy changes associated with NB adsorption on a specific adsorbent (Ag-rGO).[70] By manipulating the temperature in eq 19, we determined the thermodynamic distribution coefficient (K_d) or equilibrium distribution constant (K_{eq}).

$$K_d = \frac{C_{\text{adsorbed}}}{C_e} \tag{18}$$

$$\Delta G = -RT \ln\left(\frac{q_e}{C_e}\right) \tag{19}$$

$$\Delta G = \Delta H - T\Delta S \tag{20}$$

The experimental concentrations of adsorbate adsorbed (C_{adsorbed}) over the sorbent/Ag-rGO and the unadsorbed adsorbate remaining in the bulk solution at equilibrium were determined at various temperatures, and the values were subsequently calculated using eq 19.[72] These K_{eq} values were then used to calculate the ΔG for the adsorption. Likewise, ΔH and ΔS values were obtained from the intercept and slope of the plot for ΔG versus temperature, as indicated in Figure 8d, respectively. Table 4 presents the values of the essential parameters related to thermodynamics. The Gibbs free energy change (ΔG) was found to be negative at all temperatures, proving the adsorption process's viability and spontaneity. The ΔG values dropped as the temperature increased, indicating that low temperatures are more beneficial for the adsorption processes.[1] The negative ΔG values are also supported by the negative ΔH and positive ΔHS values during the dye removal process. In addition, this trend not only indicates the spontaneous nature of the adsorption process but also indicates that Ag-rGO is a good adsorbent for the NB removal process. The mean value of the enthalpy change (ΔH) is a measure of the energetic changes that occur between the bulk solution and surface of the solid adsorbent. In other words, it indicates the measure of energy changes that are needed to overcome the energy barrier faced by the adsorbate molecules in going from the bulk of the solution to the surface of the solid adsorbent. The negative values of ΔH indicate that the adsorption is exothermic in nature. Hence, it suggests that the extent of the adsorption process reduces with an increase in the experimental temperature. On the basis of our previous knowledge understanding, it can be said that the values of change in the entropy (ΔS) indirectly indicate whether the adsorption process is occurring through an associative or dissociative mechanism. It is generally expected that dissociative mechanism (more randomness) dominates when the value ΔS is positive, while for the negative value of ΔS, an associative mechanism (less randomness) is expected. In the present case, the positive ΔS value suggests that some structural changes may occur in the structure of adsorbate and adsorbent during the adsorption process. The fact that ΔS is positive implies that there is a rise in randomness at the solid-solution interface during the NB adsorption process. However, it can be seen that the values of ΔS are much smaller as compared to the ΔG and ΔH. These results demonstrate that the adsorption of NB over the surface of Ag-rGO adsorbent is a typical spontaneous process, which is an enthalpy and to some extent the entropy-driven adsorption process in nature.

3.6. Summary on the Effectiveness of Ag-rGO Composite toward NB Removal under Different Experimental Variables and Possible Interactions.
Due to the presence of finely sized silver nanoparticles (Ag) and reduced graphene oxide (rGO), it is expected that Ag-rGO composite possesses appreciable surface area and abundant adsorption sites for attachment of external molecules. Nile blue dye molecules initially adsorb onto the surface of the composite through various interactions, such as $\pi-\pi$ stacking, electrostatic attraction, and hydrogen bonding between the dye molecules and the functional groups present on the surface of Ag-rGO nanohybrid. In addition to the higher surface area, the Ag-rGO is expected to have a porous structure due to the presence of reduced graphene oxide. This structure offers appropriate active sites for the adsorption of the Nile blue dye molecules. It is also supposed that NB dye molecules can undergo $\pi-\pi$ stacking interactions with the aromatic rings of graphene sheets in rGO. Additionally, electrostatic forces may happen between the positively charged nitrogen atoms in the dye molecules and the negatively charged oxygen-containing functional groups on the surface of Ag-rGO. The possible existence of oxygen-containing functional groups (e.g., hydroxyl, carboxyl, epoxy) on the surface of adsorbent can also enhance the adsorption process through hydrogen bonding and other chemical forces between the NB molecule and adsorbent surface. Different aspects such as composite composition and the ratio of silver nanoparticles to reduced graphene oxide in the composite can affect the photocatalytic activity and adsorption capacity. Optimum ratios can result in an increased removal efficiency. In addition, incident light intensity can also affect the production of reactive oxygen species (ROS) within the composite, thus quickening the photoassisted removal of NB. As discussed in the earlier

Scheme 5. Schematic Representation of the Mechanism for the Removal of NB Dyes using Ag-rGO Nanocomposite
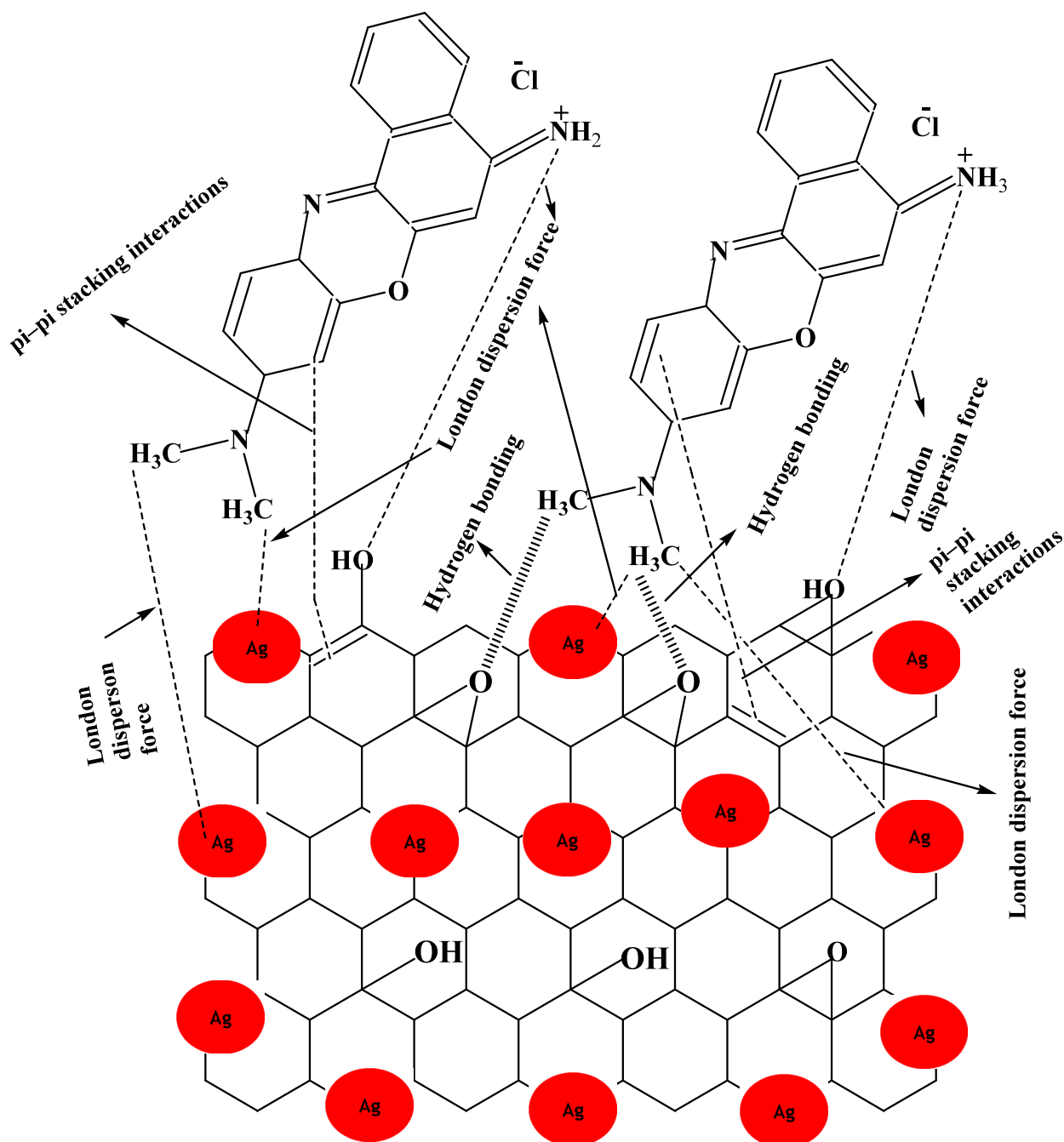
section, pH affects the surface charge of the Ag-rGO material and the charge of the dye molecules. Optimal pH conditions can increase electrostatic forces and amend dye adsorption. Likewise, the pH can also impact the chemical stability of the material and the dye molecules, affecting the complete removal efficiency. Likewise, a suitable ratio of NB to Ag-rGO is also important for effective outcomes. Experimental temperature also has a visible effect on this removal process; as higher temperatures can increase the mass transfer rate of dye molecules to the composite surface and modify reaction kinetics, resulting in faster removal rates. Furthermore, temperature can also affect the thermal stability of the material and degradation intermediates, possibly influencing the overall removal effectiveness. The presence of coexisting ions or organic compounds in the solution may strive with dye molecules for adsorption sites or react with ROS, affecting the removal proficiency. Also, increased agitation or mixing can amend the contact between the composite and dye molecules, simplifying adsorption and photocatalytic degradation processes. In the NB removal process, the type and strength of interactions between the dye molecules and the surface of Ag-rGO are of prime importance, because higher interaction leads to greater adsorption. The pictorial representation of the possible interactions is summarized in Scheme 5.

3.7. Summary on the Comparative Effectiveness of the Present Materials toward the Removal of Dye with Earlier Reports. To facilitate comprehension of the current study, a concise comparison is provided between the present

Table 5. Brief Comparison of the Dye Removal Efficiency of the Present Materials with That in the Previous Literature

material	dye	experimental conditions	adsorption capacity (mg/g)/% removal	reference
GO	NB	material dose = 0.01 g, t = 60 min, conc = 20 mg/L, sol = 20 mL, T = 30 °C, pH = 6	8.8/22%	this work
rGO	NB	material dose: 0.01 g, t: 60 min, conc: 20 mg/L, sol: 20 mL, T: 30 °C, pH: 6	20/50%	this work
Ag-rGO	NB	material dose: 0.01 g, t: 60 min, conc: 20 mg/L, sol: 20 mL, T: 30 °C, pH: 6	36.8/92%	this work
Ag-rGO + light	NB	material dose = 0.01 g, t = 60 min, conc = 20 mg/L, sol = 20 mL, T = 30 °C, pH = 6	38/95%	this work
Ma/rGO	NB	material = 0.1 g, t = 60 min, conc = 20 mg/L, sol = 50 mL, T = 90 °C, pH = 6	35.2/95%	73
Cu_2O/rGO	NB	material = 0.1 g, t = 60 min, conc = 25 mg/L, sol = 50 mL, T = 90 °C, pH = 7	9.83/94.7%	74
Au@Ni/rGO	NB	material = 0.1 g, t = 120 min, conc = 25 mg/L, sol = 50 mL, T = 45 °C, pH = 4	20/93%	75
Ag/rGO	MO	material = 0.4 g, t = 60 min, conc = 100 mg/L, sol = 50 mL, T = 45 °C, pH = 5.5	14.9/91%	76
Ag/$CuFe_2O_4$/rGO	MB/MO	material = 0.5 g, t = 60 min, conc = 75 mg/L, sol = 25 mL, T = 30 °C, pH = 9	3.71/99%	77
AgNP/rGO	MB	material = 0.8 g, t = 50 min, conc = 10 mg/L, sol = 25 mL, T = 45 °C, pH = 2	29.9/99.98%	78
Ag@RGO/g-C_3N_4	AM	material = 0.2 g, t = 20 min, conc = 100 mg/L, sol = 50 mL, T = 25 °C, pH = 7	24.8/93%	79
Ag/rGO	MB	material = 0.5 g, t = 30 min, conc = 20 mg/L, sol = 30 mL, T = 40 °C, pH = 5	16.5/99%	65
Ag/rGO	CR	material = 0.5 g, t = 120 min, conc = 100 mg/L, sol = 50 mL, T = 40 °C, pH = 5	12.4/93.65%	80
Ag/rGO	SO	material = 0.3 g, t = 60 min, conc = 200 mg/L, sol = 50 mL, T = 35 °C, pH = 7	28.5/96%	81
Ni–Co–S/SDS	CV, Rh B, MB, NB MO and CR and Cr(VI)	adsorbent = 5 mg, conc = 10 to 5000 mg/L, sol = 50 mL, T = 25 °C, pH = 7	4417.79, 3556.04, 1451.64, 773.47, 3598.23, 3284.08, and 583.67	33
MoO_3/Ppy	NB	adsorbent = 0.5 g, T = 30 °C, conc = 0.5 mg/L, sol = 500 mL, t = 15 min, T = 25 °C, pH = 7	181 and 189	29
hydroxyapatite@Mn–Fe	Cr(VI) and NB	composite dosage = 1.5 and 1 g, for Cr(VI) and NB, t = 5–130 min, conc = 10–100 mg/L, T = 25 °C, pH = 2 and 10	97.63 and 98.83%	32
carboxymethyl cellulose-*graft*-poly(methacrylic acid-co-acrylamide)/kaolin nanocomposite	NB	adsorbent = 1.5 mg, conc = 10 ppm, T = 25 °C, t = 90 min, pH = 11	96.49–98.91%	82
GG-PAAm/Er_2O_3NC	NB	adsorbent = 0.8 g, pH = 6, T = 313 K, t = 40 min, C = 80 mg/L		83
$CuWO_4$	NB	adsorbent = 400 mg, T = 30 °C, C = 10 μM/L		84
Ni–Co–S@Ct	MB, CV, NB, CR As(III), and As(V)	adsorbent = mg, C = 10 to 5000 mg/L, pH = 8, T = 25 °C	4417.79, 3556.04, 1451.64, 773.47, 3598.23, 3284.08, and 583.67	31
AC	NB	T = 500 °C	99.56 and 85.23	85
AC/$CoFe_2O_4$	MB, MV, NB	adsorbent = 0.1 g, t = 40 min, T = 25 °C, C = 10 mg/L, pH = 8 and 9	86.24, 83.90, and 87.48	40
MWCNTs	NB			86
Zeolite clay/Fe–Al LDH	MV and NB	adsorbent = 1 g, t = 40 min, T = 25 °C, pH = 9	81.98 and 60.61/99.14 and 98.67%	28
CNT/MgO/$CuFe_2O_4$	MVD and NBD	adsorbent = 1 g, t = 40 min, T = 25 °C, C = 10 mg/L, pH = 2–8	36.46 and 35.60	30
clay and clay/starch/$MnFe_2O_4$	MY and NB	adsorbent = 0.2–2 g, t = 5–200 min, T = 25–50 °C, C = 10–140 mg/L, pH = 2–10	67.82 and 72.25	42
CuO–SiO_2	NB	adsorbent = 0.1 g, t = 5–200 min, T = 25 °C, C = 20 mg/L, pH = 8	70%	61
CuO–SiO_2/PVA	NB and MB	adsorbent = 0.1 g, t = 300 and 360 min, T = 25 °C, C = 20 mg/L, pH = 8	58 and 51%	87
g-C_3N_4/$ZnCo_2O_4$	MB	adsorbent = 90 mg, T = 25 °C, C = 5 mg/L	99%	88

adsorbents and those documented in the prior literature for the removal of a specific dye. Additionally, the efficacy of similar adsorbents toward structurally different dyes is also presented. Table 5 presents a comparative analysis of the dye removal capacities of the current adsorbents (GO, rGO, and Ag-rGO) with those of previously published materials. Upon comparison with other adsorbents documented in the literature, it becomes evident that all three adsorbents, namely, GO, rGO, and Ag-rGO, exhibit remarkable performance in dye removal process. Overall, the results reveal that adsorption efficacy changes with variation in experimental factors such as the adsorbent type and amount, pollutant concentration, contact time, pH, and temperature. This is because that in the dye removal process (adsorptive or catalysis), the dye first comes to the surface of the material/adsorbent and attaches to it via some intermolecular forces (Hydrogen bonding, London dispersion forces, and/or electrostatic forces etc.). Normally, a dynamic equilibrium is established between dye molecules in the bulk and at the surface of the adsorbent, leading to the removal of the dye from wastewater. As a result, the chemical composition, diverse textures, and morphological features of the adsorbent play significant roles in its efficacy in wastewater treatment. These results indicate that current carbon-based adsorbents show remarkable activity in removing organic contaminants over a shorter period. Furthermore, this adsorptive and potential catalytic property can be further enhanced by modifying this carbon-based nanomaterial from graphite to graphene oxide (GO), from GO to reduced graphene oxide (rGO), and from rGO to silver-decorated reduced graphene oxide (Ag-rGO). This improvement in desirable applications can be accredited to variations in the chemical composition, texture and morphological properties, bandgap energies, etc., achieved by inexpensive and more practicable modification approaches.

3.8. Summary of Advantages and Limitations of the Current Study. This study primarily focuses on comparing and evaluating the efficacy of graphene oxide (GO), reduced graphene oxide (rGO), and silver-decorated reduced graphene oxide (Ag-rGO), for removing hazardous pollutants such as Nile blue (NB) dye from aqueous environments. The investigation involves analyzing their chemical composition, structure, and morphology. The findings reveal that modifying GO/rGO-based materials with silver (Ag) effectively transfers desirable properties of Ag to GO/rGO, achieved through a well-established and cost-effective method known as the one-pot simple hydrothermal approach. The method used here not only is simpler but also reduces complexity and cost as compared to other sophisticated approaches. The integration of Ag nanoparticles into rGO to create Ag-rGO via a one-pot hydrothermal method is expected to positively impact the adsorption capabilities of rGO. Additionally, significant reusability of the Ag-rGO nanocomposite, attributed to minimal Ag leaching and good stability, was observed.

Regarding limitations, the study focused on the removal of NB dye through batch approaches, but real textile water samples may contain other potential pollutants and ions. Therefore, exploring the potential applications of our fabricated materials for treating real wastewater samples from various textile industries should be addressed in future studies. Additionally, proper strategies should be designed for the disposal and/or reuse of the adsorbent after the dye removal process.

4. CONCLUSIONS

In this work, we have successfully fabricated graphene oxide (GO), reduced graphene oxide (rGO), and silver-decorated reduced graphene oxide (Ag-rGO)-based materials using a low-cost, one-pot hydrothermal approach, and their chemical, structural, and morphological behavior were assessed from spectroscopic techniques. Afterward, their adsorptive efficiencies for the removal of toxic Nile blue dye from wastewater were investigated. The Nile blue removal performance of all of the fabricated materials (i.e., GO, rGO, and Ag-rGO) was evaluated by varying the adsorbent amount, dye concentration, pH of the medium, and experimental temperature. The Ag-rGO nanocomposite samples were found to exhibit exceptional performance, achieving a maximum dye removal rate of 94% (20 mg/L) within 60 min, whereas only 50 and 22% of Nile blue (NB) were removed by rGO and GO, respectively. In the case of Ag-rGO, the dye removal efficiency was found to be higher at a greater Ag loading in the composite. After analyzing the adsorption data through thermodynamics, isotherms, and kinetic models, we observed that the Ag-decorated rGO samples had an effective adsorption capacity favored by the thermodynamic and kinetic properties of the adsorption process. Furthermore, the possible interactions of NB dye with these modified carbon-based materials might be collective physicochemical interactions, such as van der Waals forces, hydrogen bonding, and electrostatic interactions. These interactions can be altered by changing the pH of the medium, as well. Additionally, it was found that the presence of light enhanced the adsorptive removal of Nile blue (NB) dye when Ag-rGO was used as an adsorbent. Thermodynamic results demonstrated that the adsorption of NB over the surface of the Ag-rGO adsorbent is a typical spontaneous process, which is an enthalpy and to some extent the entropy-driven adsorption process in nature. Appreciable reusability of the Ag-rGO nanocomposite was observed in the present study, which can be attributed to negligible Ag leaching and/or good stability of the Ag-rGO composite under the experimental conditions used. Based on the overall observations, it can be said that silver-decorated carbon-based nanocomposites demonstrate appreciable and cost-effective potential for wastewater decontamination. This study offers valuable insights into the development of binary and ternary nanocomposites for potential catalytic applications and, especially, efficient adsorptive and catalytic applications.

■ AUTHOR INFORMATION

Corresponding Authors

Abbas Khan — *Department of Chemistry, Abdul Wali Khan University Mardan, Mardan 23200, Pakistan; Energy, Water and Environment Lab, College of Humanities and Sciences, Prince Sultan University, Riyadh 11586, Saudi Arabia;* Email: abbas80@awkum.edu.pk

Muhammad Humayun — *Energy, Water and Environment Lab, College of Humanities and Sciences, Prince Sultan University, Riyadh 11586, Saudi Arabia;* orcid.org/0000-0003-3504-3935; Email: mhumayun@psu.edu.sa

Authors

Natasha — *Department of Chemistry, Abdul Wali Khan University Mardan, Mardan 23200, Pakistan*

Ubaid Ur Rahman — *Department of Chemistry, Abdul Wali Khan University Mardan, Mardan 23200, Pakistan*

Sadaf − *Department of Chemistry, Abdul Wali Khan University Mardan, Mardan 23200, Pakistan*

Muhammad Yaseen − *Department of Chemistry, Abdul Wali Khan University Mardan, Mardan 23200, Pakistan*

Rasha A. Abumousa − *Energy, Water and Environment Lab, College of Humanities and Sciences, Prince Sultan University, Riyadh 11586, Saudi Arabia*

Rozina Khattak − *Department of Chemistry, Shaheed Benazir Bhutto Women University Avenue, Peshawar 00384, Pakistan;* orcid.org/0000-0001-5196-3331

Noor Rehman − *Department of Chemistry, Shaheed Benazir Bhutto University, Dir Upper 18000, Pakistan*

Mohamed Bououdina − *Energy, Water and Environment Lab, College of Humanities and Sciences, Prince Sultan University, Riyadh 11586, Saudi Arabia*

Complete contact information is available at:
https://pubs.acs.org/10.1021/acsomega.4c00973

Author Contributions

All authors have contributed to this study at different stages. N., A.K., and M.H. were responsible for study design, method design, analytical protocol design, writing, reviewing, and editing. M.H., S., and A.K. were responsible for experimental assistant, discussion during writing, and reviewing. U.U.R. and M.Y. were responsible for experimental assistant and data analysis. R.K., N.R., A.K., R.A.A., M.B., and M.H. were responsible for reviewing and editing. All authors read and approved the final version of this manuscript.

Notes

The authors declare no competing financial interest.

■ REFERENCES

(1) Alam, S.; Khan, M. S.; Umar, A.; Khattak, R.; ur Rahman, N.; Zekker, I.; Burlakovs, J.; Rubin, S. S. D.; Ghangrekar, M. M.; Bhowmick, G. D.; Kallistova, A.; Pimenov, N.; Khan, A.; Zahoor, M. Preparation of Pd−Ni nanoparticles supported on activated carbon for efficient removal of basic blue 3 from water. *Water* **2021**, *13* (9), 1211.

(2) Mahar, I.; Mahar, F. K.; Mahar, N.; Memon, A. A.; Pirzado, A. A. A.; Khatri, Z.; Thebo, K. H.; Ali, A. Fabrication and characterization of MXene/carbon composite-based nanofibers (MXene/CNFs) membrane: An efficient adsorbent material for removal of Pb^{+2} and As^{+3} ions from water. *Chem. Eng. Res. Des.* **2023**, *191*, 462−471.

(3) Khan, A.; Noor, S.; Khan, M.; Khattak, R.; Malik, A.; Rahman, U.; Zekker, I.; Rahman, N.; Shah, L. Removal of crystal violet from wastewater using synthesized graphene quantum dots as adsorbents: Kinetic approach. *Int. J. Environ. Sci. Technol.* **2023**, *11*, 1−14.

(4) Shahzad, M. K.; Memon, F. H.; Soomro, F.; Iqbal, M.; Ibrar, A.; Memon, A. A.; Lim, J. H.; Choi, K. H.; Thebo, K. H. MoS$_2$-based lamellar membranes for mass transport applications: Challenges and opportunities. *J. Environ. Chem. Eng.* **2023**, *11* (2), No. 109329.

(5) Rehman, F.; Memon, F. H.; Ullah, S.; Mazumder, M. A. J.; Al-Ahmed, A.; Khan, F.; Thebo, K. H. Recent Development in Laminar Transition Metal Dichalcogenides-Based Membranes Towards Water Desalination: A Review. *Chem. Rec.* **2022**, *22* (9), No. e202200107.

(6) Mangalam, J.; Kumar, M.; Sharma, M.; Joshi, M. High adsorptivity and visible light assisted photocatalytic activity of silver/reduced graphene oxide (Ag/rGO) nanocomposite for waste-water treatment. *Nano-Struct. Nano-Objects.* **2019**, *17*, 58−66.

(7) Gupta, D. K.; Rajaura, R. S.; Sharma, K.; Jasuja, N. D.; Sharma, K. Synthesis and characterization of graphene oxide nanoparticles and their antibacterial activity. *Int. J. Environ. Sci. Technol.* **2015**, *1* (1), 16−24.

(8) George, D.; James, G.; Manjally, J. K.; Thomas, J.; Kuriakose, M. S.; Aryamol, K.; Benny, A.; George, S. C. Graphene/PANI electrode material characterization for supercapacitor application. *Mater. Today Proc.* **2020**, *24*, 1734−1741.

(9) Tarcan, R.; Todor-Boer, O.; Petrovai, I.; Leordean, C.; Astilean, S.; Botiz, I. Reduced graphene oxide today. *J. Mater. Chem. C* **2020**, *8* (4), 1198−1224.

(10) Trikkaliotis, D. G.; Mitropoulos, A. C.; Kyzas, G. Z. Low-cost route for top-down synthesis of over-and low-oxidized graphene oxide. *Colloids Surf. A: Physicochem. Eng. Asp.* **2020**, *600*, No. 124928.

(11) Yu, X.; Zhang, W.; Zhang, P.; Su, Z. Fabrication technologies and sensing applications of graphene-based composite films: advances and challenges. *biosens. bioelectron.* **2017**, *89*, 72−84.

(12) Ikram, M.; Raza, A.; Imran, M.; Ul-Hamid, A.; Shahbaz, A.; Ali, S. Hydrothermal synthesis of silver decorated reduced graphene oxide (rGO) nanoflakes with effective photocatalytic activity for wastewater treatment. *Nanoscale Res. Lett.* **2020**, *15*, 1−11.

(13) Abu-Nada, A.; Abdala, A.; McKay, G. Removal of phenols and dyes from aqueous solutions using graphene and graphene composite adsorption: a review. *J. Environ. Chem. Eng.* **2021**, *9* (5), No. 105858.

(14) Humayun, M.; Bahadur, A.; Khan, A.; Bououdina, M. Exceptional Photocatalytic Performance of the LaFeO$_3$/g-C$_3$N$_4$ Z-Scheme Heterojunction for Water Splitting and Organic Dyes Degradation. *Catal.* **2023**, *13* (5), 907.

(15) Malik, A.; Khan, A.; Anwar, N.; Naeem, M. A comparative study of the adsorption of Congo red dye on rice husk, rice husk char and chemically modified rice husk char from aqueous media. *Bull. Chem. Soc. Ethiopia* **2020**, *34* (1), 41−54, DOI: 10.4314/bcse.v34i1.4.

(16) Affat, S. S. Classifications, advantages, disadvantages, toxicity effects of natural and synthetic dyes: a review. *Univ. Thi-Qatar J. Sci.* **2021**, *8* (1), 130−135.

(17) Mehra, S.; Singh, M.; Chadha, P. Adverse impact of textile dyes on the aquatic environment as well as on human beings. *Toxicol. Int.* **2021**, *28* (2), 165.

(18) Ji, J.; Yuan, X.; Zhao, Y.; Jiang, L.; Wang, H. Mechanistic insights of removing pollutant in adsorption and advanced oxidation processes by sludge biochar. *J. Hazard. Mater.* **2022**, *430*, No. 128375.

(19) Karthik, C.; Swathi, N.; Caroline, D. G. Green synthesized rGO-AgNP hybrid nanocomposite—an effective antibacterial adsorbent for photocatalytic removal of DB-14 dye from aqueous solution. *J. Environ. Chem. Eng.* **2020**, *8* (1), No. 103577.

(20) Vijina, C.; Damodaran, S. P. Platinum nanoparticle-decorated reduced graphene oxide nanosheets: A recyclable and highly efficient catalyst towards the reduction of para-nitrophenol and methylene blue. *Results Eng.* **2023**, *20*, No. 101444.

(21) Kar, P.; Sardar, S.; Liu, B.; Sreemany, M.; Lemmens, P.; Ghosh, S.; Pal, S. K. Facile synthesis of reduced graphene oxide−gold nanohybrid for potential use in industrial waste-water treatment. *Sci. Technol. Adv. Mate.* **2016**, *17* (1), 375−386.

(22) Elbakry, S.; Ali, M. E.; Abouelfadl, M.; Badway, N. A.; Salam, K. M. Photocatalytic degradation of organic compounds by TFC membranes functionalized with Ag/rGO nanocomposites. *J. Photochem. Photobiol. A: Chem.* **2022**, *430*, No. 113957.

(23) Qazi, U. Y.; Iftikhar, R.; Ikhlaq, A.; Riaz, I.; Jaleel, R.; Nusrat, R.; Javaid, R. Application of Fe-RGO for the removal of dyes by catalytic ozonation process. *Environ. Sci. Pollut. Res.* **2022**, *29* (59), 89485−89497.

(24) Nasrollahzadeh, M.; Jaleh, B.; Baran, T.; Varma, R. S. Efficient degradation of environmental contaminants using Pd-RGO nano-

composite as a retrievable catalyst. *Clean Technol. Environ. Policy.* **2020**, *22*, 325−335.

(25) Mondal, S.; Patel, S.; Majumder, S. K. Bio-extract assisted in-situ green synthesis of Ag-RGO nanocomposite film for enhanced naproxen removal. *Korean J. Chem. Eng.* **2020**, *37*, 274−289.

(26) Al-Assaly, R.; Al-Nafiey, A. Synthesize rGO-Ag NPs nanocomposite by a simple physical method and applying in water treatment. *AIP Conf. Proc.* **2022**, *2386*, No. 080030.

(27) Mamo, B. Y.; Zeleke, T. D. Green synthesis of rGO/Ag nanocomposite using extracts of Cinnamomum verum plant bark: Characterization and evaluation of its application for Methylene blue dye removal from aqueous solutions. *Int. J. Nano Dimens.* **2022**, *13* (4), 414−434.

(28) Kamali, M.; Esmaeili, H.; Tamjidi, S. Synthesis of zeolite clay/Fe-Al hydrotalcite composite as a reusable adsorbent for adsorption/desorption of cationic dyes. *Arab. J. Sci. Eng.* **2022**, *47* (5), 6651−6665.

(29) Siddiqui, M. F.; Khan, E. A.; Khan, T. A. Synthesis of MoO_3/polypyrrole nanocomposite and its adsorptive properties toward cadmium (II) and nile blue from aqueous solution: equilibrium isotherm and kinetics modeling. *Environ. Prog. Sustainable Energy* **2019**, *38* (6), No. e13249.

(30) Foroutan, R.; Peighambardoust, S. J.; Esvandi, Z.; Khatooni, H.; Ramavandi, B. Evaluation of two cationic dyes removal from aqueous environments using $CNT/MgO/CuFe_2O_4$ magnetic composite powder: A comparative study. *J. Environ. Chem. Eng.* **2021**, *9* (2), No. 104752.

(31) Sajid, M.; Sharma, A.; Choudhry, A.; Chaudhry, S. A. Synthesis, Characterization and potential application of functionalised binary metallic sulphides for water reclamation. *Colloids Surf. C* **2023**, No. 100011.

(32) Alali, A. F.; Almojil, S. F.; Almohana, A. I.; Anqi, A. E.; Rajhi, A. A.; Alamri, S.; Dhahad, H. A. Hydroxyapatite@Mn−Fe composite as a reusable sorbent for removal of Nile blue dye and Cr(VI) from polluted water. *Environ. Sci. Pollut. Res.* **2023**, *30* (7), 18419−18437.

(33) Chowdhury, A.; Khan, A. A.; Kumari, S.; Hussain, S. Super adsorbent Ni−Co−S/SDS Nanocomposites for Ultrahigh Removal of Cationic, Anionic Organic Dyes and Toxic Metal Ions: Kinetics, Isotherm and Adsorption Mechanism. *ACS Sustain. Chem. Eng.* **2019**, *7* (4), 4165−4176.

(34) Du, Y.; Wang, J.; Zou, Y.; Yao, W.; Hou, J.; Xia, L.; Peng, A.; Alsaedi, A.; Hayat, T.; Wang, X. Synthesis of molybdenum disulfide/reduced graphene oxide composites for effective removal of Pb (II) from aqueous solutions. *Sci. Bull.* **2017**, *62* (13), 913−922.

(35) Zhou, S.; Gao, J.; Wang, S.; Fan, H.; Huang, J.; Liu, Y. Highly efficient removal of Cr (VI) from water based on graphene oxide incorporated flower-like MoS_2 nanocomposite prepared in situ hydrothermal synthesis. *Environ. Sci. Pollut. Res.* **2020**, *27*, 13882−13894.

(36) Abedinpour, S.; Mahkam, M.; Zonouz, A. M. Graphenic molybdenum disulfide nanocomposites as heterogeneous nanocatalyst for reduction of nitroanilines. *J. Photochem. Photobiol. A: Chem.* **2024**, *448*, No. 115281.

(37) Trang, P. T. T.; Tam, T. T.; Vien, V.; Lien, N. H. Application of MoS_2/reduced graphene oxide for photocatalytic degradation of rhodamine B in water environment. *IOP Conference Series:Mater. Sci. Eng.* **2020**, *902*, No. 012041.

(38) Verma, S.; Pandey, C. M.; Kumar, D. A highly efficient rGO grafted MoS_2 nanocomposite for dye adsorption and electrochemical detection of hydroquinone in swastewater. *New J. Chem.* **2022**, *46* (44), 21190−21200.

(39) Mohd Norsham, I. N. Molybdenum disulphide/ reduced graphene oxide (MOS_2/RGO) hybrid for photo degradation of perfluorooctanoic acid (PFOA) in aqueous solution (Doctoral dissertation, Universiti Teknologi MARA (UiTM)). 2023.

(40) Foroutan, R.; Mohammadi, R.; Ramavandi, B. Elimination performance of methylene blue, methyl violet, and Nile blue from aqueous media using $AC/CoFe_2O_4$ as a recyclable magnetic composite. *Environ. Sci. Poll. Res.* **2019**, *26*, 19523−19539.

(41) Alipour, N.; Namazi, H. Removing Paraquat and Nile blue from aqueous solution using double-oxidized graphene oxide coated by polydopamine nanocomposite. *Int. J. Environ. Sci. Technol.* **2019**, *16* (7), 3203−3210.

(42) Esvandi, Z.; Foroutan, R.; Peighambardoust, S. J.; Akbari, A.; Ramavandi, B. Uptake of anionic and cationic dyes from water using natural clay and clay/starch/$MnFe_2O_4$ magnetic nanocomposite. *Surf. Interfaces.* **2020**, *21*, No. 100754.

(43) Kamali, M.; Esmaeili, H.; Tamjidi, S. Synthesis of Zeolite Clay/Fe-Al Hydrotalcite Composite as a Reusable Adsorbent for Adsorption/Desorption of Cationic Dyes. *Arabian J. Sci. Eng.* **2022**, *47* (5), 6651−6665.

(44) Ikram, M.; Ilyas, B.; Haider, A.; Haider, J.; Ul-Hamid, A.; Shahzadi, A.; Goumri-Said, S.; Kanoun, M. B.; Nabgan, W.; Mahmood, A. Fabrication of La-Doped MoS_2 Nanosheets with Tuned Bandgap for Dye Degradation and Antimicrobial Activities, Experimental and Computational Investigations. *Adv. Mater. Interfaces* **2023**, 2202404.

(45) Khan, M.; Ikram, M.; Haider, A.; Ul-Hamid, A.; Ullah, H.; Shahzadi, I.; Khan, S.; Kanoun, M. B.; Goumri-Said, S.; Medina, F.; Nabgan, W. Experimental and DFT study of GO-decorated CaO quantum dots for catalytic dye degradation and bactericidal potential. *Front. Environ. Sci.* **2023**, *11*, 1158399.

(46) Haldorai, Y.; Shim, J. J. An efficient removal of methyl orange dye from aqueous solution by adsorption onto chitosan/MgO composite: A novel reusable adsorbent. *Appl. Surf. Sci.* **2014**, *292*, 447−453.

(47) Gong, J. L.; Wang, X. Y.; Zeng, G. M.; Chen, L.; Deng, J. H.; Zhang, X. R.; Niu, Q. Y. Copper (II) removal by pectin−iron oxide magnetic nanocomposite adsorbent. *J. Chem. Eng.* **2012**, *185*, 100−107.

(48) Ren, Y.; Abbood, H. A.; He, F.; Peng, H.; Huang, K. Magnetic EDTA-modified chitosan/SiO_2/Fe_3O_4 adsorbent: preparation, characterization, and application in heavy metal adsorption. *J. Chem. Eng.* **2013**, *226*, 300−311.

(49) Khan, T. A.; Nazir, M.; Ali, I.; Kumar, A. Removal of chromium (VI) from aqueous solution using guar gum−nano zinc oxide biocomposite adsorbent. *Arab. J. Chem.* **2017**, *10*, S2388−S2398.

(50) Chen, J.; Feng, J.; Yan, W. Influence of metal oxides on the adsorption characteristics of PPy/metal oxides for Methylene Blue. *J. Colloid Interface Sci.* **2016**, *475*, 26−35.

(51) Li, X.; Lu, H.; Zhang, Y.; He, F. Efficient removal of organic pollutants from aqueous media using newly synthesized polypyrrole/$CNTs$-$CoFe_2O_4$ magnetic nanocomposites. *J. Chem. Eng.* **2017**, *316*, 893−902.

(52) Li, J.; Feng, J.; Yan, W. Synthesis of polypyrrole-modified TiO_2 composite adsorbent and its adsorption performance on acid red G. *J. Appl. Polym. Sci.* **2013**, *128* (5), 3231−3239.

(53) Calimli, M. H.; Nas, M. S.; Burhan, H.; Mustafov, S. D.; Demirbas, Ö.; Sen, F. Preparation, characterization and adsorption kinetics of methylene blue dye in reduced-graphene oxide supported nanoadsorbents. *J. Mol. Liq.* **2020**, *309*, No. 113171.

(54) Gupta, D. K.; Rajaura, R. S.; Sharma, K. Synthesis and characterization of graphene oxide nanoparticles and their antibacterial activity. *Int. J. Environ. Sci. Technol.* **2015**, *1* (1), 16−24.

(55) Yaseen, M.; Humayun, M.; Khan, A.; Idrees, M.; Shah, N.; Bibi, S. Photo-Assisted Removal of Rhodamine B and Nile Blue Dyes from Water Using CuO−SiO_2 Composite. *Molecules.* **2022**, *27* (16), 5343.

(56) Priya, V. S.; Basha, S. K.; Kumari, V. S. Kinetics and adsorption performance of biosorbent starch/poly(vinyl alcohol)/graphene oxide nanocomposite for the removal of dyes. *J. Umm Al-Qura Univ. Appl. Sci.* **2023**, *9* (4), 529−547.

(57) Qusti, A. H.; Mohamed, R. M.; Salam, M. A. Photocatalytic synthesis of aniline from nitrobenzene using Ag-reduced graphene oxide nanocomposite. *Ceram. Int.* **2014**, *40* (4), 5539−5546.

(58) Minh Dat, N.; Linh, V. N. P.; Huy, L. A.; Huong, N. T.; Tu, T. H.; Phuong, N. T. L.; Nam, H. M.; Thanh Phong, M.; Hieu, N. H. Fabrication and antibacterial activity against Pseudomonas aeruginosa and Staphylococcus aureus of silver nanoparticle decorated reduced

graphene oxide nanocomposites. *Mater.Technol.* **2019**, *34* (7), 369–375.

(59) Sharif, S.; Ahmad, K. S.; Memon, F. H.; Rehman, F.; Soomro, F.; Thebo, K. H. Functionalised graphene oxide-based nanofiltration membranes with enhanced molecular separation performance. *Mater. Res. Innov.* **2022**, *26* (6), 373–381.

(60) Thiyagarajulu, N.; Arumugam, S.; Narayanan, A. L.; Mathivanan, T.; Renuka, R. R. Green synthesis of reduced graphene nanosheets using leaf extract of tridax procumbens and its potential in vitro biological activities. *Biointerface Res. Appl. Chem.* **2020**, *11*, 9975–9984.

(61) Yaseen, M.; Farooq, S.; Khan, A.; Shah, N.; Shah, L. A.; Bibi, S.; Khan, I. U.; Ahmad, S. CuO-SiO₂ based nanocomposites: Synthesis, characterization, photocatalytic, antileishmanial, and antioxidant studies. *J. Chin. Chem. Soc.* **2022**, *69* (9), 1637–1653.

(62) Khune, A. S.; Padghan, V.; Bongane, R.; Narwade, V. N.; Dole, B.; Ingle, N. N.; Tsai, M.-L.; Hianik, T.; Shirsat, M. D. Highly Selective Chemiresistive SO₂ Sensor Based on a Reduced Graphene Oxide/Porphyrin (rGO/TAPP) Composite. *Electron. Mater.* **2023**, *52* (12), 8108–8123.

(63) Alduwaib, S. M.; Abd, M. M. Investigating the Structural, Optical and Antibacterial Properties of GO, GO: Ag, GO: ZnO Thin Layers and GO: ZnO/GO: Ag Bilayers Synthesized by Spray Pyrolysis Method. *Iran. J. Mater. Sci. Eng.* **2020**, *17* (4), 170 DOI: 10.22068/ijmse.17.4.170.

(64) Devendran, P.; Selvakumar, D.; Ramadoss, G.; Sivaramakrishnan, R.; Alagesan, T.; Jayavel, R.; Pandian, K. A novel visible light active rare earth doped CdS nanoparticles decorated reduced graphene oxide sheets for the degradation of cationic dye from wastewater. *Chemosphere.* **2022**, *287*, No. 132091.

(65) Dat, N. M.; Long, P. N. B.; Nhi, D. C. U.; Minh, N. N.; Duy, L. M.; Quan, L. N.; Nam, H. M.; Phong, M. T.; Hieu, N. H. Synthesis of silver/reduced graphene oxide for antibacterial activity and catalytic reduction of organic dyes. *Synth. Met.* **2020**, *260*, No. 116260.

(66) Karthikeyan, P.; Nikitha, M.; Pandi, K.; Meenakshi, S.; Park, C. M. Effective and selective removal of organic pollutants from aqueous solutions using 1D hydroxyapatite-decorated 2D reduced graphene oxide nanocomposite. *J. Mol. Liq.* **2021**, *331*, No. 115795.

(67) Wu, Z.; Yuan, X.; Zhong, H.; Wang, H.; Jiang, L.; Zeng, G.; Wang, H.; Liu, Z.; Li, Y. Highly efficient adsorption of Congo red in single and binary water with cationic dyes by reduced graphene oxide decorated NH₂-MIL-68 (Al). *J. Mol. Liq.* **2017**, *247*, 215–229.

(68) Kahsay, M. H.; Belachew, N.; Tadesse, A.; Basavaiah, K. Magnetite nanoparticle decorated reduced graphene oxide for adsorptive removal of crystal violet and antifungal activities. *RSC Adv.* **2020**, *10* (57), 34916–34927.

(69) Ismail, H. K.; Ali, L. I. A.; Alesary, H. F.; Nile, B. K.; Barton, S. Synthesis of a poly (p-aminophenol)/starch/graphene oxide ternary nanocomposite for removal of methylene blue dye from aqueous solution. *J. Polym. Res.* **2022**, *29* (5), 159.

(70) Rahman, U. U.; Humayun, M.; Khan, A.; Farooq, S.; Sadiq, M.; Bououdina, M.; Shah, N. Thermo-Chemical Modification of Cellulose for the Adsorptive Removal of Titan Yellow from Wastewater. *Molecules.* **2023**, *28* (9), 3955.

(71) Zhang, X.; Ma, C.; Wen, K.; Han, R. Adsorption of phosphate from aqueous solution by lanthanum modified macroporous chelating resin. *Korean J. Chem. Eng.* **2020**, *37*, 766–775.

(72) Vidovix, T. B.; Quesada, H. B.; Bergamasco, R.; Vieira, M. F.; Vieira, A. M. S. Adsorption of Safranin-O dye by copper oxide nanoparticles synthesized from Punica granatum leaf extract. *Environ. Technol.* **2022**, *43* (20), 3047–3063.

(73) Minati, L.; Speranza, G.; Micheli, V.; Dalla Serra, M.; Clamer, M. Graphene oxide nanocomposite magnetic microbeads for the remediation of positively charged aromatic compounds. *Dalton Trans.* **2020**, *49* (10), 3333–3340.

(74) Saigl, Z. M. Various adsorbents for removal of Rhodamine B dye: A review. *Indones. J. Chem.* **2021**, *21* (4), 1039–1056.

(75) Ren, G.; Han, H.; Wang, Y.; Liu, S.; Zhao, J.; Meng, X.; Li, Z. Recent advances of photocatalytic application in water treatment: A review. *Nanomater.* **2021**, *11* (7), 1804.

(76) Mangalam, J.; Kumar, M.; Sharma, M.; Joshi, M. High adsorptivity and visible light assisted photocatalytic activity of silver/reduced graphene oxide (Ag/rGO) nanocomposite for wastewater treatment. *Nano-Struct. Nano-Objects.* **2019**, *17*, 58–66.

(77) Nirumand, L.; Farhadi, S.; Zabardasti, A. Magnetically separable Ag/CuFe₂O₄/reduced Graphene oxide ternary Nanocomposite with high performance for the removal of Nitrophenols and dye pollutants from aqueous media. *Acta Chim. Slov.* **2018**, *65* (4), 919–931.

(78) Sodeinde, K. O.; Olusanya, S. O.; Enogheghase, V. F.; Lawal, O. S. Photocatalytic degradation of Janus Green Blue dye in wastewater by green synthesised reduced graphene oxide-silver nanocomposite. *Int. J. Environ. Anal. Chem.* **2022**, *103*, 1–17, DOI: 10.1080/03067319.2021.2002309.

(79) Hamza, M. A.; Abd El-Rahman, S. A.; El-Shazly, A. N.; Hashem, E. M.; Mohamed, R. T.; El-Tanany, E. M.; Elmahgary, M. G. Facile one-pot ultrasonic-assisted synthesis of novel Ag@ RGO/g-C₃N₄ ternary 0D@ 2D/2D nanocomposite with enhanced synergetic tandem adsorption-photocatalytic degradation of recalcitrant organic dyes: Kinetic and mechanistic insights. *Mater. Res. Bull.* **2021**, *142*, No. 111386.

(80) Borthakur, P.; Boruah, P. K.; Hussain, N.; Silla, Y.; Das, M. R. Specific ion effect on the surface properties of Ag/reduced graphene oxide nanocomposite and its influence on photocatalytic efficiency towards azo dye degradation. *Appl. Surf. Sci.* **2017**, *423*, 752–761.

(81) Thakur, K.; Kandasubramanian, B. Graphene and graphene oxide-based composites for removal of organic pollutants: a review. *J. Chem. Eng. Data* **2019**, *64* (3), 833–867.

(82) Jafarian, E.; Hekmatiyan, A.; Cheraghdar, A.; Safarzadeh, H.; Shamsi, M. Elimination performance of Nile blue from wastewater using by carboxymethyl cellulose-graft-poly (methacrylic acid-co-acrylamide)/kaolin nanocomposite hydrogel. *Int. J. Environ. Sci. Technol.* **2023**, *20* (9), 9933–9944.

(83) Hussain, D.; Khan, S. A.; Khan, T. A.; Alharthi, S. S. Efficient liquid phase confiscation of nile blue using a novel hybrid nanocomposite synthesized from guar gum-polyacrylamide and erbium oxide. *Sci. Rep.* **2022**, *12* (1), 14656.

(84) Kavitha, B.; Karthiga, R. Synthesis and characterization of CuWO₄ as nano-adsorbent for removal of Nile blue and its antimicrobial studies. *J. Mater. Environ. Sci.* **2020**, *11*, 57–68.

(85) Hamad, K. H.; El-Sayed, A. M.; Mohamed, A. G.; Mostafa, A. H.; Deeb, N. M. E.; Tedawy, A. H.; Leithy, A. G. E.; Abdelhamid, M. F.; Tawab, S. A.; Aly, S. T. Synthesis of Activated Carbon from Agricultural Wastes and Its Application in Adsorption of Dyes. *Chem. Eng. Technol.* **2023**, *46* (9), 1876–1885.

(86) Ghoochian, M. Adsorption of Nile blue A from wastewater using magnetic multi-walled carbon nanotubes: Kinetics and equilibrium studies. *Iran. J. Toxicol.* **2016**, *10* (3), 7–12.

(87) Yaseen, M.; Khan, A.; Humayun, M.; Bibi, S.; Farooq, S.; Bououdina, M.; Ahmad, S. Fabrication and characterization of CuO–SiO₂/PVA polymer nanocomposite for effective wastewater treatment and prospective biological applications. *Green Chem. Lett. Rev.* **2024**, *17*, 1.

(88) Hai, T.; Chaturvedi, R.; Mostafa, L.; Kh, T. I.; Soliman, N. F.; El-Shafai, W. Designing g-C₃N₄/ZnCo₂O₄ nanocomposite as a promising photocatalyst for photodegradation of MB under visible-light excitation: response surface methodology (RSM) optimization and modeling. *J. Phys. Chem. Solids.* **2024**, *185*, No. 111747.